

Composing Linear Layers from Irreducibles

Travis Pence Daisuke Yamada Vikas Singh

University of Wisconsin-Madison
 {tnpence, dyamada2}@wisc.edu, vsingh@biostat.wisc.edu

Abstract

Contemporary large models often exhibit behaviors suggesting the presence of low-level primitives that compose into modules with richer functionality, but these fundamental building blocks remain poorly understood. We investigate this compositional structure in linear layers by asking: *can we identify/synthesize linear transformations from a minimal set of geometric primitives?* Using Clifford algebra, we show that linear layers can be expressed as compositions of bivectors—geometric objects encoding oriented planes—and introduce a differentiable algorithm that decomposes them into products of rotors. This construction uses only $\mathcal{O}(\log^2 d)$ parameters, versus $\mathcal{O}(d^2)$ required by dense matrices. Applied to the key, query, and value projections in LLM attention layers, rotor-based layers match the performance of strong baselines such as block-Hadamard and low-rank approximations. Our findings provide an algebraic perspective on how these geometric primitives can compose into higher-level functions within deep models.

1 Introduction

There is growing consensus [Kozachkov et al., 2023] that, like biological systems, modern models may internally rely on *low-level primitives* that *compose* to form modules with more complex functionality [Weiss et al., 2021]. This compositional perspective was one motivation behind capsule networks [Sabour et al., 2017], which explicitly modeled part-whole relationships through vector-based capsules. But the task of localizing and characterizing such primitives remains challenging albeit interesting. A general capability to compose pre-trained modules in a prescribed way could, in principle, lead to a larger model with predictable and more controllable functionality [Zou et al., 2025, Schug et al., 2024, Ghazi et al., 2019, Abnar et al., 2023, Press et al., 2023], with potential applications ranging from safety guardrails to interpretability.

Some recent results suggest some progress in this direction. In mixture-of-experts architectures [Masoudnia and Ebrahimpour, 2014, Riquelme et al., 2021], specialized sub-networks are conditionally activated and composed via routing [Büchel et al., 2025]. Model merging has evolved from simple parameter averaging to more sophisticated alignment of different model latent representations [Lähner and Moeller, 2024]. Fine-tuning methods like LoRA [Hu et al., 2021] implicitly assume that low-dimensional adjustment of a base network should suffice—essentially a two-level composition. Each approach offers a distinct perspective on composition (e.g., see Chytas et al. [2024]) but are not focused on addressing how the mechanistic composition of low-level primitives gives more complex behavior. To this end, mechanistic interpretability [Rai et al., 2024] and neurosymbolic methods [Yang and Chaudhuri, 2022] explore this space, but are still in a nascent stage of development.

Scope of this paper. Consider a core module—with millions of parameters—in a large model. *Can we synthesize its functionality from its most basic primitives? How many such objects would we need?* This casts our broader interest in composition into a concrete problem: *identifying a minimal set of irreducibles that combine in specific ways to realize the full functionality of the module.* We study this problem for *linear layers*—noting that linear layers make up a large portion of parameters in large

language models (LLMs). While prior work suggests various parameter-efficient approximations, our interest is not only function approximation, rather to build up the functionality by characterizing its *algebraic structure*. To formalize the above intuition, we use the language of *Clifford algebra*, where linear transformations naturally decompose into simple *bivectors*—geometric objects representing oriented planes. This view reveals how the functionality of a linear layer can be synthesized as a structured composition of a few hundred geometric objects (parameters).

Our key **contributions** are: **(a)** We express linear transformations as compositions of geometric primitives—specifically, bivectors in Clifford algebra—using rotor sandwich products acting on local subspaces of an input multivector. This requires $\mathcal{O}(\log^2 d)$ scalar parameters, compared to $\mathcal{O}(d^2)$ for dense layers, where d is the input/output dimension. **(b)** We propose a differentiable invariant decomposition algorithm that maps bivectors to their corresponding rotors in closed-form, which enables integration with autograd and gradient-based optimization. **(c)** Empirically, we replace the key, query, and value projections in LLM attention layers and show comparable downstream performance in accuracy and perplexity across various datasets.

Our goal is to show the *feasibility* of this algebraic decomposition approach. It is not a drop-in replacement yet, since practical benefits will require additional system-level integration beyond the scope of this work. The focus here is on the underlying algorithmic and mathematical foundations.

2 Preliminaries

We review some relevant concepts from Clifford algebra (also see Hestenes and Sobczyk [2012]).

Clifford algebra. A *Clifford algebra*, $\text{Cl}_{p,q}(\mathbb{R})$, is an associative algebra over \mathbb{R}^n equipped with a quadratic form of signature (p, q) , where $n = p + q$. The algebra admits two basic products: the *inner product* and *outer (wedge) product*, denoted by \cdot and \wedge respectively. Their sum defines the *geometric product*, which for vectors $u, v \in \mathbb{R}^n$ takes the form:

$$uv \triangleq u \cdot v + u \wedge v.$$

The algebra is generated by orthogonal basis vectors e_1, \dots, e_n , called *generators*, satisfying:

$$e_i^2 = +1 \quad \text{for } 1 \leq i \leq p; \quad e_j^2 = -1 \quad \text{for } p < j \leq n; \quad e_i \wedge e_j = -e_j \wedge e_i \quad \text{for } i \neq j.$$

These relations encode the metric and orientation of the underlying space. The algebra has a canonical basis of 2^n elements: the scalar 1 and all distinct products of the basis vectors e_1, \dots, e_n . In particular, *basis bivectors* are wedge products of two distinct basis vectors, i.e., $e_i \wedge e_j = e_i e_j$ for $i < j$. More generally, *basis k-vectors* are wedge products of k distinct basis vectors (see Fig. 1), and there are $\binom{n}{k}$ such elements for each k . The total number of such basis elements is the *dimension* of the algebra. The *reversion*, given by \dagger , reverses the order of basis vectors. For example, $(e_1 e_2)^\dagger = e_2 e_1$ and $(e_1 e_2 e_3)^\dagger = e_3 e_2 e_1$.

The algebra decomposes into a direct sum of subspaces indexed by *grade*: scalars (grade 0), vectors (grade 1), *bivectors* (grade 2), and general *k-vectors*, which are linear combinations of corresponding basis elements. A *multivector* is a general element of $\text{Cl}_{p,q}(\mathbb{R})$, expressed as a linear combination of components of multiple grades. For example, $e_1 e_2$ is a basis bivector; $e_1 e_3 + 2e_2 e_3$ is a bivector; and $1 + (2e_2 + e_4) - e_1 e_3$ is a multivector composed of elements of grades 0, 1, and 2. We denote the subspaces of vectors and bivectors by $\text{Cl}^1(\mathbb{R})$ and $\text{Cl}^2(\mathbb{R})$, and more generally, $\text{Cl}^k(\mathbb{R})$ for grade- k elements. The algebra naturally splits into *even* and *odd* subalgebras based on grade parity. The *even subalgebra* $\text{Cl}^+(n) \subset \text{Cl}(n)$ consists of elements of even grade (scalars, bivectors, 4-vectors, etc), while odd elements include vectors, trivectors, and so on. Some well-known algebraic systems arise as special cases of Clifford algebras: the real numbers $\mathbb{R} \cong \text{Cl}_{0,0}(\mathbb{R})$, the complex numbers $\mathbb{C} \cong \text{Cl}_{0,1}(\mathbb{R})$, the quaternions $\mathbb{H} \cong \text{Cl}_{0,2}(\mathbb{R})$, and the hyperbolic numbers $\text{Cl}_{1,0}(\mathbb{R})$. This way, Clifford algebras naturally generalize familiar algebraic systems by incorporating geometric structure. To keep notations short, we write $\text{Cl}_{p,q}(\mathbb{R})$ as $\text{Cl}(p, q)$ and only consider $\text{Cl}(n, 0)$, denoted as $\text{Cl}(n)$.

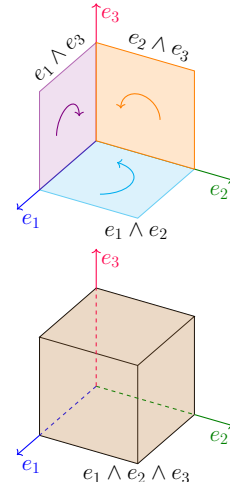


Figure 1: The basis vectors, bivectors, and trivector for $\text{Cl}(3)$. The top part shows a 3D coordinate system with basis vectors e_1 (blue), e_2 (green), and e_3 (red). It highlights three bivectors: $e_1 \wedge e_2$ (purple plane), $e_2 \wedge e_3$ (orange plane), and $e_1 \wedge e_3$ (cyan plane). The bottom part shows a 3D cube representing the trivector $e_1 \wedge e_2 \wedge e_3$.

3 Algebraic Structure of Rotor-based Transformations

We aim to describe standard linear transformations in terms of the algebraic structure of Clifford algebra. We begin by noting how any linear map can be expressed as a sum of multivector products, and then show how restricting to rotors in the Spin group is helpful.

Clifford form of linear transformations. A linear map between two vector spaces is one that preserves additivity and homogeneity. Traditionally, such transformations are represented as dense matrices with independent parameters. In contrast, we consider $\text{Cl}(n)$ and write these transformations in terms of the geometric product between multivectors—algebraic objects that encode both magnitude and orientation. We first restate a textbook result.

Lemma 1. (Hestenes and Sobczyk [2012]) *Let a_t and b_t denote multivectors in $\text{Cl}(n)$. Any linear function F from $\text{Cl}^k(n)$ to $\text{Cl}(n)$ can be written as the finite sum for some width $w < \infty$,*

$$F(x) = \sum_{t=1}^w a_t x b_t. \quad (1)$$

This result shows that linear transformations in Clifford algebra can be expressed as products involving multivectors acting from both the left and right. Thus, Clifford algebra gives us a way to represent a general, arbitrary linear map. But there is a cost: arbitrary multivectors have too much freedom and require all 2^n parameters of the full Clifford algebra, which makes the representation inefficient. We will constrain a_t and b_t to preserve *rotational symmetries*, leading to the Spin group

$$\text{Spin}(n) \triangleq \{r \in \text{Cl}^+(n) \mid rr^\dagger = 1\}$$

where $\text{Cl}^+(n) \subset \text{Cl}(n)$ is the even subalgebra and \dagger denotes grade-wise reversion. The Spin group captures the set of orientation-preserving rotations within $\text{Cl}(n)$. The elements $r \in \text{Spin}(n)$, called *rotors*, act on multivectors $x \in \text{Cl}(n)$ through the sandwich product as shown in Fig. 2,

$$x \mapsto rxr^\dagger. \quad (2)$$

Applying multiple rotors in *parallel* instantiates Lem. 1, where $a_t = r_t$ and $b_t = r_t^\dagger$. We clarify that while the *general* Clifford algebra can represent any linear map, restricting to $\text{Spin}(n)$ limits transformations to orthogonal (rotation-preserving) ones. Consequently, our construction does not capture arbitrary linear maps. In practice, expressivity is recovered by combining multiple rotor modules acting on different subspaces and aggregating their outputs (see Sec. 5). While this sandwich form is useful, we must efficiently parametrize these rotors. To do so, we first observe the relationship between $\text{Spin}(n)$ and the more familiar rotation group, $\text{SO}(n)$.

Fact 1 (Gallier and Quaintance [2020]). *$\text{Spin}(n)$ is a double cover of the special orthogonal group $\text{SO}(n)$ for $n \geq 3$.*

This relationship is important in that while $\text{Spin}(n)$ and $\text{SO}(n)$ are topologically different (hence the “double cover”), they share the same infinitesimal structure—namely, their Lie algebra. This allows using parametrization techniques for $\text{SO}(n)$ to represent elements of $\text{Spin}(n)$. In particular, we will see that rotors can be generated from bivectors via the exponential map, just as rotation matrices arise from skew-symmetric matrices.

Remark. *For vector inputs x , the sandwich product rxr^\dagger performs the same rotation as the corresponding matrix in $\text{SO}(n)$. However, the full utility of rotors becomes clear when x is multivector: the transformation extends to higher-grade components within the Clifford algebra, going beyond the vector subspace. This makes rotors especially suitable for operating on the richer representations.*

We return to the question: can we efficiently represent rotors so that a_t, b_t in Lem. 1 belong to $\text{Spin}(n)$?

Constructing rotors from bivectors. *Rotors in $\text{Spin}(n)$ can be parametrized via bivectors:* grade-2 elements of $\text{Cl}(n)$ that encode oriented planes of rotation. To understand this parametrization, we examine the connection between rotors and rotation matrices via Lie groups and their Lie algebras.

Definition 1. *A Lie group G is a smooth manifold with the usual group properties along with smooth (infinitely differentiable) group operations. Its associated Lie algebra is a vector space equipped with an antisymmetric, bilinear operation $[X, Y]$, called the Lie bracket, satisfying the Jacobi identity.*

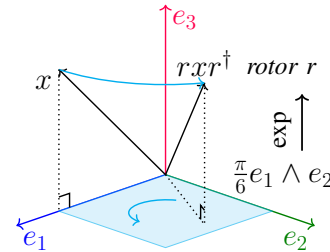


Figure 2: The sandwich product rotating a vector 60° in the $e_1 \wedge e_2$ plane.

Let us check examples. $\text{Spin}(n)$ and $\text{SO}(n)$ are different Lie groups with the same Lie algebra. Specifically, the Lie algebra of skew-symmetric matrices, $\mathfrak{so}(n) \triangleq \{B \in \mathbb{R}^{n \times n} | B = -B^T\}$, underlies both $\text{Spin}(n)$ and $\text{SO}(n)$, despite their topological differences. This shared structure is important. The exponential map gives a surjective correspondence between $\mathfrak{so}(n)$ to $\text{SO}(n)$ as

$$\exp(B) = \sum_{i=0}^{\infty} \frac{B^i}{i!}, \quad (3)$$

showing that every rotation in $\text{SO}(n)$ can be realized as $\exp(B)$ for some $B \in \mathfrak{so}(n)$ using only $\dim(\mathfrak{so}(n)) = \binom{n}{2}$ independent parameters—fewer than the n^2 entries of a matrix [Lezcano-Casado and Martínez-Rubio, 2019]. The bridge to the Clifford algebra setting is from another key isomorphism:

Fact 2 (Doran and Lasenby [2003]). *The space of skew-symmetric matrices is isomorphic to that of bivectors, i.e., $\mathfrak{so}(n) \cong \text{Cl}^2(n)$.*

Given a skew-symmetric matrix $B \in \mathfrak{so}(n)$, the corresponding bivector $b \in \text{Cl}^2(n)$ is constructed as

$$b = \sum_{1 \leq i < j \leq n} B_{i,j} e_i \wedge e_j.$$

Similar to the exponential map relating $\mathfrak{so}(n)$ and $\text{SO}(n)$ (i.e., $\exp(B)$ generating rotations in $\text{SO}(n)$), every rotor $r \in \text{Spin}(n)$ is the exponential of some bivector $b \in \text{Cl}^2(n)$ given explicitly by the series

$$r = \exp(b) = \sum_{i=0}^{\infty} \frac{b^i}{i!}, \quad (4)$$

where b^k is the k -fold geometric product of b with itself. This means that we can encode a rotor with only $\dim(\text{Cl}^2(n)) = \binom{n}{2}$ parameters—the dimension of the bivector space.

Main advantage. At first glance, our parametrization may seem to offer no advantage. We have parametrized both $\text{Spin}(n)$ and $\text{SO}(n)$ from the same $\binom{n}{2}$ parameters from $\mathfrak{so}(n)$. Notice that while $\text{SO}(n)$ acts only on n -dimensional vectors, rotors in $\text{Spin}(n)$ act on a subset of the full 2^n -dimensional space of multivectors. By utilizing *rotors as the action on multivector input and bivectors as our irreducible primitives*, we will use exponentially fewer parameters.

Example 3.1. A $d \times d$ dense matrix with $d = 2048$, common in self-attention blocks and projection layers (e.g., in LLaMa), uses more than 4M parameters. If w (e.g., $\simeq 3$) is the width hyperparameter in Lem. 1, approximating with bivector irreducibles requires only $w \left(\log_2 d \right) = 55 w$.

This reduction (to 55×3) comes from identifying bivectors as the primitive that generate rich linear maps through composition. Note that the infinite series in (4) is problematic due to the need for approximation. We avoid this by presenting a closed-form solution that preserves differentiability.

4 Algorithmic Implementation and Analysis of our Rotor-gadget

We discussed above how rotors can be parametrized through bivectors via the exponential map in (4). A remaining challenge is the infinite series. Of course, we can truncate to a finite length and incur approximation errors. However, for a special class of bivectors, the exponential map admits an exact closed-form solution, which prevents any approximation errors. Moreover, this form remains fully differentiable. We describe the details of this alternative here.

4.1 Closed-form differentiable computations of rotors

A key observation is that when a skew-symmetric matrix $B \in \mathfrak{so}(n)$ generates a rotation restricted to a single 2-dimensional plane, the matrix exponential in (3) reduces to a finite closed-form expression—mirroring the simplicity of the classic Rodrigues formula for axis-angle rotations [Goldstein et al.,

Algorithm 1 Differentiable Inv. Decomp.

Require: $b \in \text{Cl}^2(n)$, $v \in \text{Cl}^1(n)^{k-1}$
Ensure: Inv. Decomp. $\{b_1, \dots, b_k\}$,
singular vectors $\{v_1, \dots, v_{k-1}\}$
1: Initialize **decomp**, **vectors** $\leftarrow \emptyset, \emptyset$
2: **for** $i = 1$ to $k-1$ **do**
3: $b_s, v_i \leftarrow \text{Proj}_{\text{simple}}(b, v_i)$
4: $b \leftarrow b - b_s$
5: **decomp** $\leftarrow \text{decomp} \cup \{b_s\}$
6: **vectors** $\leftarrow \text{vectors} \cup \{v_i\}$
7: **end for**
8: **decomp** $\leftarrow \text{decomp} \cup \{b\}$
9: **return** **decomp**, **vectors**

Algorithm 2 GA Power Iteration

Require: $b \in \text{Cl}^2(n)$, $v \in \text{Cl}^1(n)$,
threshold $\epsilon \in \mathbb{R}$
Ensure: Approximate $\text{Proj}_{\text{simple}}(b)$
1: $v_{\text{prev}} \leftarrow v$
2: **while** $\|v + v_{\text{prev}}\| > \epsilon$ **do**
3: $v_{\text{prev}} \leftarrow v$
4: $v \leftarrow b \llcorner (b \llcorner v)$
5: $v \leftarrow v / \|v\|_2$
6: **end while**
7: $\sigma u = b \llcorner v$
8: $b_s \leftarrow \sigma u \wedge v$
9: **return** b_s, v

2002]. An analogous simplification holds for bivectors. The exponential map in (4) admits a closed form when $b \in \text{Cl}^2(n)$ is *simple*, meaning it can be written as $b = u \wedge v$ for some vectors $u, v \in \text{Cl}^1(n)$, or equivalently $b \wedge b = 0$. This ensures that b represents a single-plane rotation rather than a composition of rotations. The resulting closed-form expression is:

$$\exp(b) = \cos(\|b\|) + \frac{\sin(\|b\|)}{\|b\|} b. \quad (5)$$

This form is exact [Doran and Lasenby, 2003]. However, restricting to simple bivectors is limiting, as simple bivectors span only a *subset* of $\text{Cl}^2(n)$, and thus generate only a *subset* of $\text{Spin}(n)$. To capture the full expressivity of rotor-based transformations, we wish to extend to general bivectors.

Building bivectors from simple bivectors. To utilize the closed-form exponential in (5) while retaining the full richness of $\text{Cl}^2(n)$, we need a way to express arbitrary bivectors in terms of simple ones. Fortunately, Roelfs and Keninck [2021] show that any bivector $b \in \text{Cl}^2(n)$ admits an *invariant decomposition* as a sum of at most $k \triangleq \lfloor n/2 \rfloor$ mutually commuting, orthogonal, simple bivectors $\{b_1, b_2, \dots, b_k\}$. This decomposition has two key advantages: (1) each component b_i admits an efficient closed-form solution $\exp(b_i)$ in (5) since b_i is simple, and (2) mutual commutativity ensures $\exp\left(\sum_{i=1}^k b_i\right) = \prod_{i=1}^k \exp(b_i)$, via the standard Lie algebra identity $\exp(X + Y) = \exp(X) \exp(Y)$ when their commutator $[X, Y] = 0$. In $\mathfrak{so}(n)$, the Lie bracket is $[X, Y] = XY - YX$, which vanishes when X and Y commute. With these benefits in place, the remaining question is how to construct the decomposition? A recent result provides a spectral formulation in terms of the eigenvectors and eigenvalues of b , stated below.

Lemma 2 (Thm. 4.8 in Eelbode et al. [2024]). *Let $b \in \text{Cl}^2(n)$ have as many eigenvectors as its effective pseudo-dimension. Then, we have*

$$b = \sum_{j=1}^k \mu_j \frac{v_{\mu_j^+} \wedge v_{\mu_j^-}}{v_{\mu_j^+} \cdot v_{\mu_j^-}},$$

where $\sigma(b) = \{\pm \mu_1, \dots, \mu_k\}$ is the spectrum of b and $v_{\mu_j^+}$ and $v_{\mu_j^-}$ are partner eigenvectors.

Differentiable invariant decomposition. While the invariant decomposition can be computed using eigendecomposition, standard algorithms pose challenges. The eigenvalues of a bivector come in conjugate pairs, and singular values come in positive pairs, making differentiation (and backpropagation) not as straightforward due to the numerical instability of eigen-decomposition for near-degenerate singular values. To address this, we introduce a Krylov subspace-inspired algorithm that iteratively extracts the simple bivectors without requiring explicit eigendecomposition. The procedure is shown in Alg. 1. It includes a subroutine for projecting a bivector onto the manifold of simple bivectors, which we accomplish with a Clifford algebraic adaptation of the power iteration method shown in Alg. 2. This uses right contraction $b \llcorner v$, which extracts the components of b that lie in the direction of v , avoiding the need to construct explicit matrix representations.

The projection has the closed-form expression $\text{Proj}_{\text{simple}}(b) = \sigma(u \wedge v)$ where σ is the top singular value of b , and u, v are the corresponding left and right singular vectors. Note that because of sign symmetry of the paired singular vectors, we detect convergence by the sum, not their difference, and threshold ϵ . Further discussion and proofs of Alg. 1–2 are in Appendix B. We provide a full visualization of bivector to rotor in Fig. 3.

Computation graph size. To control the size of the computation graph, we adapt DEQ [Bai et al., 2019]: we run the fixed-point iteration without gradient tracking, and then perform a single final forward pass with tracking enabled. This ensures that the graph scales only with k (number of components in decomposition), and not the number of iterations in Alg. 2, which depends on the spectral gap and threshold ϵ . Also, while one could initialize v in Alg. 2 using a non-differentiable SVD, this is unnecessary. Under small perturbations of b , the singular vectors vary smoothly. This follows from matrix perturbation results, which guarantees that in non-degenerate cases, eigenspaces vary analytically with the matrix entries (Ch. 2 of Kato [1980]). Thus, warm-starting with the previous singular vectors yields fast convergence, if gradient steps are not too large.

4.2 A Generalized Rotor Gadget

Occasionally, we may need mappings between arbitrary dimensional spaces. To do so, we now describe a generalized rotor gadget. Instead of the standard sandwich product in (2), we can allow two different rotors on left/right for more expressiveness. Define the rotor-based transformation as:

$$\psi_{r,s}(x) \triangleq rxs^\dagger, \quad (6)$$

where $r, s \in \text{Spin}(n)$. This construction, however, assumes the linear map acts on data with dimension of the Clifford algebra, a power of 2. To address this, we use multiple rotor-sandwich modules operating on different subspaces. For arbitrary input and output dimensions d_{in} and d_{out} , we utilize the rotor-sandwich modules $\psi_{r,s}(x)$ as building blocks to construct a map $\psi : \mathbb{R}^{d_{\text{in}}} \rightarrow \mathbb{R}^{d_{\text{out}}}$. Fix positive integers c_1, c_2 , and n with $2^n \leq \min(d_{\text{in}}, d_{\text{out}})$ and let $[h] \triangleq \{1, 2, \dots, h\}$. For each $i \in [c_1]$ and $j \in [c_2]$, define $I_i \subseteq [d_{\text{in}}]$ and $O_j \subseteq [d_{\text{out}}]$ as 2^n subsets of input and output coordinates, respectively. We associate each pair with a rotor map $\psi_{r_{ij}, s_{ij}}$ defined by rotors $r_{ij}, s_{ij} \in \text{Spin}(n)$, parametrized by their corresponding bivectors $a_{ij}, b_{ij} \in \text{Cl}^2(n)$. Then, each sub-module operates on $\text{Cl}(n)$ and computes the rotor-sandwich action $\psi_{r_{ij}, s_{ij}} : \mathbb{R}^{I_i} \rightarrow \mathbb{R}^{O_j}$. The full output is defined by aggregating all $c_1 c_2$ rotor maps:

$$\psi(x) \triangleq \sigma \left(\left\{ \psi_{r_{ij}, s_{ij}}(x^{I_i}) \mid i \in [c_1], j \in [c_2] \right\} \right), \quad (7)$$

where σ is a pooling operator on the outputs of $\psi_{r_{ij}, s_{ij}}$. Note that $\cup_i I_i = [d_{\text{in}}]$ and $\cup_j O_j = [d_{\text{out}}]$ are needed to fully cover the input and output dimensions. This gives us a general rotor-based transformation from arbitrary input and output dimensions parametrized by bivectors which is visualized in Fig. 4. We now analyze the number of learnable parameters ψ requires.

Theorem 1 (ψ Parameter Count). *Let $\psi : \mathbb{R}^{d_{\text{in}}} \rightarrow \mathbb{R}^{d_{\text{out}}}$ be the mapping defined above, composed of rotor modules $\psi_{r_{ij}, s_{ij}}$ with $i \in [c_1]$ and $j \in [c_2]$, each acting in $\text{Cl}(n)$ with $2^n \leq \min(d_{\text{in}}, d_{\text{out}}) \triangleq d$. The total number of learnable parameters is upper bounded by*

$$2c_1 c_2 \binom{n}{2} = \mathcal{O}(\log^2 d).$$

Thm. 1 shows that rotor maps use only $\mathcal{O}(\log^2 \min(d_{\text{in}}, d_{\text{out}}))$ parameters. In comparison, a standard dense layer and rank- r factorization require $\mathcal{O}(d_{\text{in}} d_{\text{out}})$ and $\mathcal{O}(r(d_{\text{in}} + d_{\text{out}}))$, respectively.

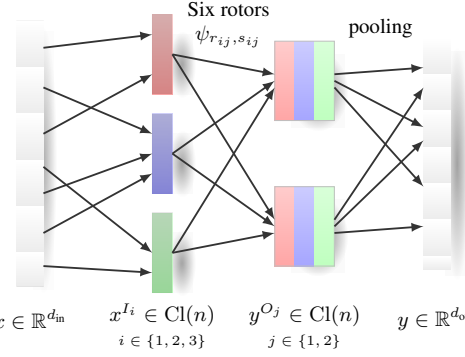


Figure 4: Rotor architecture with $c_1 = 3$ and $c_2 = 2$. An input x is split into $\{x^{I_i}\}_{i \in [c_1]}$, each mapped to y^{O_j} via rotor maps $\psi_{r_{ij}, s_{ij}}$, for each $j \in [c_2]$. The outputs $\{y^{O_j}\}$ are pooled and assembled into the final output y .

5 Experiments

Goals. We empirically evaluate rotors by *replacing key, query, and value linear layers in pre-trained LLMs* and measuring downstream performance on perplexity (PPL) and accuracy. Our experiments span multiple models and datasets. The main goals are to: **(G-1)** Demonstrate the *feasibility of composing linear layers from bivector primitives* by assessing whether rotors match baseline performance of Low-Rank and Block-Hadamard approximations across diverse settings. **(G-2)** Quantify rotor parameter efficiency compared to dense and approximate alternatives. **(G-3)** Analyze how rotor architectural choices—such as width and depth—affect performance.

We focus on linear layers in smaller pre-trained language models (up to 1.5B parameters), where reduced redundancy compared to larger models makes preserving performance harder. We do not attempt full model conversion—which would require larger calibration datasets and a layerwise optimization scheme like GPTQ [Frantar et al., 2022]. Instead, we selectively replace 1-3 attention layers (key, query, and value projections) to isolate the effect, and assess whether rotor decomposition offers competitive PPL and accuracy relative to baselines.

End-to-end training with rotors. While the main LLM experiments train rotor layers to *mimic individual dense layers in isolation* (see Sec. 5.1), we also assess their behavior when used throughout a network trained jointly from scratch. To keep the setup lightweight, we replace *all dense layers* in a simple MLP (except the classification head) with rotor layers and train the model *end-to-end* on FMNIST [Xiao et al., 2017] under identical conditions as the dense baseline. Details and results are provided in Sec. 5.2, with experimental settings in Appendix C. With this experiment, we aim to complement the layerwise LLM analysis by testing full-network training with rotor layers.

5.1 Experimental Setup

Substituting attention layers. Given $x \in \mathbb{R}^d$ to a transformer block, we have:

$$\text{Attn}(x) = \left[\text{softmax} \left(\text{mask} \left(\frac{QK^\top}{\sqrt{d}} \right) \right) V \right] W_o,$$

where the query, key, and value linear projections are defined as $Q = W_q x$, $K = W_k x$, and $V = W_v x$, with W_q , W_k , and W_v as dense learnable matrices. We *jointly* replace these linear layers in 1-3 selected attention layers with rotors or baseline approximations, *keeping other parameters fixed* except, for consistency, retraining the corresponding output linear layer W_o after each substitution.

Training protocol and architectural choices.

To fit each substitute layer (rotor, LR, or BH), we extract hidden states from the pre-trained model and minimize MSE between the projected outputs of the original and approximated layers. Each variant is trained independently using the Adam optimizer [Kingma and Ba, 2017]. In our rotor architecture, *depth* refers to the number of stacked rotor maps ψ , while *width* denotes the number of parallel rotor maps within each layer. For example, the rotor map in Fig. 4 has both width and depth equal to 1 (i.e., one rotor map). We also insert *fixed permutations* between rotors to enable grade mixing and add *normalization* layers to stabilize training; both are parameter-free. All architectural details and hyperparameters are provided in Appendix C.

	Dataset	Method	LLaMa-3.2 1B			Qwen-2.5 1.5B		
			one	two	three	one	two	three
Log-PPL	WikiText2	Original	—	2.575	—	—	2.287	—
		LR1	2.688	3.455	4.956	2.350	2.402	2.591
		LR4	2.658	2.729	2.880	2.342	2.372	2.548
		BH1	2.636	2.700	2.779	2.323	2.388	2.558
		Rotor	2.629	2.717	2.818	2.307	2.369	2.515
	C4	Original	—	3.151	—	—	2.834	—
		LR1	3.414	4.071	5.001	2.884	2.910	2.985
		LR4	3.390	3.315	3.504	2.874	2.905	2.980
		BH1	3.343	3.262	3.404	2.865	2.897	2.975
PTB	Rotor	3.261	3.285	3.428	2.854	2.900	2.977	—
		Original	—	3.260	—	—	2.985	—
		LR1	3.358	4.684	6.904	3.046	3.151	3.225
		LR4	3.316	3.400	3.466	3.034	3.127	3.192
		BH1	3.293	3.355	3.395	3.025	3.101	3.168
		Rotor	3.327	3.392	3.442	3.011	3.109	3.202
	Arc Challenge	Original	—	58.37	—	—	66.09	—
		LR1	50.78	50.44	44.26	55.06	50.97	44.55
		LR4	53.84	53.39	45.95	57.48	54.51	60.77
		BH1	54.83	54.25	49.61	60.11	49.27	60.68
Accuracy (%)	Hellaswag	Rotor	55.31	54.50	49.64	61.34	52.27	47.28
		Original	—	41.00	—	—	55.00	—
		LR1	36.17	28.93	14.47	42.53	32.33	13.93
		LR4	38.02	33.79	33.87	44.41	40.53	11.27
		BH1	39.10	35.27	35.87	45.96	42.73	13.06
		Rotor	39.33	34.94	37.52	50.20	40.60	6.868

Table 1: Log-PPL (\downarrow) and accuracy (\uparrow) using original, Low-Rank ($r = 1$ or 4), BH1, and Rotor (ours) for 1-3 layer replacements. One-layer results are averaged over all layers; two/three-layer results are averaged over five random selections. Red indicates best, blue second-best per setting.

Dataset	Method	One layer replaced (Layer index)														
		1	2	3	4	5	6	7	8	9	10	11	12	13	14	15
Wikitext2 (↓)	LR1	3.620	2.750	2.754	2.781	2.742	2.705	2.703	2.714	2.695	2.622	2.632	2.628	2.612	2.630	2.647
	LR4	3.851	2.723	2.752	2.673	2.673	2.650	2.671	2.667	2.674	2.620	2.628	2.614	2.602	2.620	2.634
	BH1	3.615	2.686	2.675	2.645	2.657	2.637	2.645	2.653	2.647	2.612	2.617	2.612	2.592	2.606	2.614
	Rotor	2.924	2.665	2.664	2.645	2.664	2.635	2.642	2.640	2.640	2.607	2.616	2.613	2.593	2.611	2.566
C4 (↓)	LR1	4.433	3.297	3.440	3.274	3.300	3.276	3.309	3.282	3.292	3.205	3.284	3.271	3.192	3.236	3.214
	LR4	4.432	3.292	3.404	3.250	3.266	3.250	3.264	3.260	3.281	3.203	3.204	3.191	3.187	3.219	3.208
	BH1	4.293	3.288	3.276	3.212	3.230	3.215	3.241	3.230	3.276	3.196	3.193	3.184	3.174	3.194	3.194
	Rotor	3.660	3.258	3.292	3.232	3.242	3.228	3.249	3.245	3.248	3.197	3.196	3.187	3.176	3.202	3.203
PTB (↓)	LR1	5.401	3.468	3.435	3.406	3.419	3.346	3.358	3.401	3.363	3.322	3.281	3.308	3.271	3.322	3.292
	LR4	5.183	3.394	3.395	3.316	3.347	3.304	3.315	3.334	3.328	3.281	3.276	3.265	3.264	3.308	3.287
	BH1	4.835	3.352	3.336	3.293	3.324	3.288	3.292	3.307	3.302	3.273	3.266	3.268	3.255	3.265	3.270
	Rotor	4.194	3.412	3.403	3.356	3.369	3.320	3.338	3.336	3.326	3.278	3.271	3.300	3.266	3.300	3.284
Arc Challenge (↑)	LR1	50.64	53.22	46.78	46.35	45.49	51.07	52.79	51.93	33.05	50.21	56.65	55.80	56.65	55.08	55.79
	LR4	50.64	53.22	50.64	51.93	54.51	55.79	54.08	51.07	46.35	51.07	58.80	59.23	57.51	56.22	57.51
	BH1	53.22	54.51	52.79	54.94	57.08	54.08	53.65	52.36	51.93	50.21	57.94	57.08	58.80	57.51	57.51
	Rotor	54.51	55.36	53.65	55.36	54.51	55.79	54.51	53.22	52.36	50.64	58.37	60.09	56.65	57.94	57.08
HellaSwag (↑)	LR1	29.00	32.00	34.33	39.67	34.00	33.00	34.00	33.00	34.67	37.00	41.00	38.33	40.33	40.00	39.67
	LR4	32.67	39.67	34.67	39.00	37.67	37.00	35.00	38.67	33.67	37.67	41.33	40.00	40.33	40.33	40.00
	BH1	37.33	37.67	37.67	41.00	37.00	40.00	40.33	37.00	36.33	36.33	42.67	40.00	41.33	42.00	41.33
	Rotor	40.00	39.67	35.67	42.33	41.00	38.67	36.67	38.67	36.00	36.67	42.00	39.67	40.33	42.00	40.67
Dataset	Method	Two layers replaced (Layer pairs)														
		10,11	10,12	10,13	10,14	10,15	11,12	11,13	11,14	11,15	12,13	12,14	12,15	13,14	13,15	14,15
Wikitext2 (↓)	LR1	2.724	2.702	2.695	2.697	2.718	2.757	2.731	2.756	2.757	2.768	2.723	2.741	2.729	2.863	2.862
	LR4	2.703	2.674	2.662	2.669	2.694	2.691	2.662	2.669	2.694	2.660	2.665	2.676	2.686	2.708	2.758
	BH1	2.677	2.660	2.645	2.650	2.656	2.670	2.643	2.662	2.660	2.645	2.656	2.657	2.655	2.680	2.700
	Rotor	2.679	2.670	2.654	2.660	2.676	2.662	2.652	2.667	2.677	2.667	2.667	2.675	2.662	2.688	2.745
C4 (↓)	LR1	3.298	3.273	3.258	3.296	3.293	3.315	3.276	3.315	3.303	3.263	3.300	3.281	3.285	3.278	3.386
	LR4	3.290	3.258	3.249	3.279	3.269	3.265	3.255	3.287	3.271	3.241	3.278	3.246	3.281	3.268	3.353
	BH1	3.281	3.241	3.228	3.246	3.244	3.242	3.227	3.246	3.244	3.216	3.237	3.226	3.234	3.232	3.296
	Rotor	3.267	3.246	3.231	3.256	3.254	3.248	3.232	3.260	3.257	3.223	3.252	3.241	3.249	3.247	3.327
PTB (↓)	LR1	3.385	3.386	3.367	3.410	3.402	3.418	3.370	3.418	3.367	3.486	3.423	3.371	3.431	3.455	3.619
	LR4	3.345	3.319	3.320	3.348	3.336	3.326	3.315	3.353	3.332	3.300	3.317	3.313	3.367	3.335	3.419
	BH1	3.315	3.307	3.297	3.304	3.310	3.309	3.287	3.332	3.301	3.281	3.293	3.298	3.294	3.300	3.345
	Rotor	3.336	3.343	3.311	3.349	3.334	3.339	3.303	3.342	3.299	3.311	3.359	3.336	3.352	3.342	3.441
Arc Challenge (↑)	LR1	43.06	46.07	46.50	48.21	43.92	46.93	55.51	57.23	55.94	52.94	54.65	54.65	54.22	55.51	54.65
	LR4	42.92	48.50	48.07	51.07	49.79	59.23	56.65	59.23	57.94	58.80	56.65	57.51	56.22	55.36	57.94
	BH1	43.35	48.50	51.07	50.21	50.64	59.66	58.37	58.80	56.65	57.94	59.23	57.51	57.94	55.65	58.37
	Rotor	45.49	48.93	53.65	52.79	51.50	57.94	57.94	58.80	56.65	59.66	56.65	57.08	57.03	55.79	57.05
HellaSwag (↑)	LR1	32.00	35.00	36.00	40.33	34.00	37.67	41.67	39.33	41.33	34.00	40.33	39.33	40.33	43.00	40.67
	LR4	32.33	35.33	38.33	38.33	36.67	39.00	41.67	41.00	42.33	40.00	38.00	39.00	40.00	39.00	37.67
	BH1	37.33	37.67	35.67	40.33	39.33	39.33	41.00	41.67	41.33	40.33	43.67	40.67	42.67	40.67	40.67
	Rotor	36.00	37.67	38.67	38.67	37.67	39.33	41.67	41.33	41.33	39.33	41.67	39.00	41.00	40.33	40.33

Table 2: Performance on log-PPL (↓) and accuracy (↑) when replacing **one attention layer (top)** for layer indices 1–15 and **two attention layers (bottom)** for pairs of indices from 10–15 of LLaMa-3.2 1B. Methods are Low-Rank ($r = 1$ and 4), BH1, and Rotor.

Models, datasets, and baselines. We evaluate on two pre-trained LLMs: LLaMa-3.2 1B [Touvron et al., 2023] and Qwen-2.5 1.5B [Qwen et al., 2025]. Metrics include log perplexity (↓) on three language modeling datasets—Wikitext2, C4 [Dodge et al., 2021], and PTB [Marcus et al., 1993]—and accuracy (↑) on two multiple-choice benchmarks—Arc Challenge [Clark et al., 2018] and HellaSwag [Zellers et al., 2019]. We compare rotors to: **(a) LR1 and LR4:** Low-rank projections with rank $r = 1$ or 4, where a dense matrix $W \in \mathbb{R}^{d_{\text{out}} \times d_{\text{in}}}$ is approximated as XY , with $X \in \mathbb{R}^{d_{\text{out}} \times r}$ and $Y \in \mathbb{R}^{r \times d_{\text{in}}}$. **(b) BH1:** Block-Hadamard [Zeng et al., 2023] of depth 1, which approximate W by BH , where H is a fixed Hadamard matrix and B is block-diagonal and learnable. Parameter counts for all the methods are detailed in Tab. 4; reference LLM performance (with dense matrices) are shown in Tab. 1. Additional experiments are provided in Appendix D.

5.2 Results and Discussion

Parameter efficiency. As shown in Tab. 4, rotors require significantly fewer parameters than both dense and approximate baselines. For example, in LLaMa-3.2 1B, the query projection uses over 4.19M parameters in its dense form, compared to 16.4K in LR4, 32.7K in BH1, and just ≤ 896 in rotors—4700 \times reduction over dense and 18 \times over LR4. Similar savings apply across key and value layers, directly supporting **G-2**.

#Epoch	1	2	3	4	5	6	7	8	9	10
Dense	85.05	86.23	87.17	88.07	87.90	88.54	89.07	89.36	89.53	89.67
Rotor	80.80	82.05	82.60	82.38	86.14	86.75	86.74	86.52	87.94	88.36

Table 3: Accuracy (%) on FMNIST over 10 epochs for dense and rotor-based MLPs.

Compute cost. Rotor layers are currently slower in wall-clock runtime. Depending on rotor width (w) and depth (d), inference is roughly $w \times d$ times slower than dense layers in our experiments. In terms of FLOPs, rotor layers require $35.8M \times (wd)$ and $82.4M \times (wd)$ on LLaMa-3.2 1B and LLaMa-3.2 3B, compared to $206.1M$ and $515.3M$ for dense layers—owing to their block-diagonal structure. These reductions arise naturally from the geometric formulation rather than from explicit sparsity constraints. During training, gradient storage and backpropagation through the decomposition (Fig. 3) add minor additional cost. Optimized kernels and hardware-aware implementations could exploit this structure much better, as well as offer memory-bandwidth benefits discussed in Sec 7.

Rotor performance vs. baselines. Despite their compact size, rotors match or outperform LR1, LR4, and BH1 across most datasets and models. In Tab. 1, on Wikitext2, rotors achieve 2.629 log-PPL in LLaMa-3.2 1B (vs. 2.636 for second-best BH1), and 2.307 in Qwen-2.5 1.5B (vs. 2.323 for second-best BH1) when a single attention layer is replaced. On Arc Challenge, rotor layers yield 55.31% accuracy in LLaMa-3.2 1B (vs. 54.83% for BH1) and 61.34% in Qwen-2.5 1.5B (vs. 57.48% for LR4). Rotor projections are consistently either the best or second-best across most settings.

Tab. 2 confirms rotor robustness across layer combinations. For example, replacing layers 12 and 13 in Qwen-2.5 1.5B yields 59.66% accuracy on Arc Challenge, outperforming LR4 (58.80%) and BH1 (57.94%). In contrast, LR1, despite having 2–5× more parameters than rotors, shows significant performance drops (e.g., log-PPL on Wikitext2 for LLaMa-3.2 1B). These results confirm **G-1** and show that rotors match downstream performance of other baselines only using far fewer parameters.

In Fig. 5, PPL consistently decreases with both increasing rotor *width* and *depth*. The strongest improvements occur from depth 1 to 2, after which gains taper off. This trend suggests that both stacking more layers (depth) and using more parallel rotor maps (width) contribute to better approximation of linear layers—showing **G-3**.

Results of end-to-end training on FMNIST. As shown in Tab. 3, the dense network improves faster in early epochs, while the rotor-based model learns more gradually but reaches a comparable final accuracy (89.67% vs. 88.36%). This suggests that end-to-end optimization with rotors is slightly slower—potentially due to the high compression—but ultimately competitive with dense layers.

Overall, the LLM results support our claim: rotor layers—constructed from bivector primitives—offer insight into how linear layers can be synthesized from a compact set of building blocks. Moreover, the FMNIST experiment shows that rotor layers are feasible when trained jointly with the rest of the network end-to-end from scratch. Our full codebase, including datasets and hyperparameters for all experiments, is available at <https://github.com/vsingh-group/ComposingLinearLayers>. Key architectural and training details are also provided in Appendix C.

6 Related Work

Compositions in machine learning. Building complex model behavior from composition of simpler compute primitives is an active research topic. Capsule networks [Sabour et al., 2017] modeled part-whole relations, while mixture-of-experts [Riquelme et al., 2021] and model merging [Lähner and Moeller, 2024] compose specialized sub-modules in a conditional manner. Recent studies show how internal circuits in LLMs organize around functional units [Weiss et al., 2021]. In NLP, Tree-structured models [Tai et al., 2015] have been used to encode syntactic composition, while works

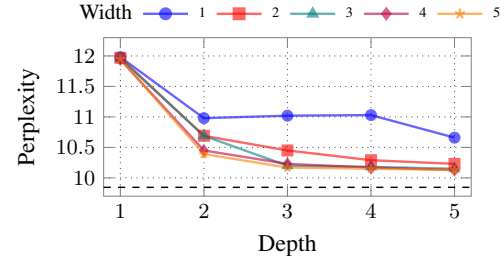


Figure 5: Effect of rotor width and depth. Replacing Layer-13 in Qwen-2.5 1.5B with rotors of varying depth and width. The dashed line (9.845) indicates convergence to the base model’s perplexity.

on compositional semantics [Mitchell and Lapata, 2008] investigate how word meanings compose to form sentence meanings. The ability to understand new combinations of familiar components remains a challenge [Zhou et al., 2024, Lake and Baroni, 2018] and a few strategies are being studied [Li et al., 2022, Chen et al., 2020, Chytas et al., 2024]. Other directions include modular approaches [Das et al., 2018, Pfeiffer et al., 2023].

Approximating linear layers. To reduce the cost of dense layers, various structured approximations are common. Low-rank factorization such as LoRA [Hu et al., 2021] constrains weights to rank- r matrices. Other matrices such as circulant [Yu et al., 2014, Cheng et al., 2015], Toeplitz [Sindhwan et al., 2015], Walsh-Hadamard [Alam et al., 2024], and Block-Hadamard [Zeng et al., 2023], among others, have been shown to be resource efficient. Our goal is to understand the compositional structure of the linear transformation itself. Resource efficiency is the *result*, not the key motivation.

Method	Key	Query	Value
Dense	1048576	4194304	1048576
LR1	2560	4096	2560
LR4	10240	16384	10240
BH1	8192	32768	8192
Rotor	≤ 1080	≤ 896	≤ 1080

Table 4: Summary of the number of parameters used for key, query, and value projections in a single attention layer of LLaMa-3.2 1B.

Clifford/Geometric algebra in ML. Recent works have explored Clifford algebra for encoding geometric structure in ML models. GCANs [Ruhe et al., 2023b] and CGENN [Ruhe et al., 2023a] construct equivariant layers by combining GA-based transformations. Clifford neural layers [Brandstetter et al., 2023] was applied to physical modeling tasks. GA has been connected to convex training of ReLU networks [Pilanci, 2024] and randomized methods for multivector representations [Wang et al., 2024] are available. GA has also been used for time-series models [Chen et al., 2025].

7 Conclusions and Future Work

We show that the functionality of standard linear layers can be expressed with exponentially fewer parameters, $\mathcal{O}(\log^2 d)$ versus $\mathcal{O}(d^2)$, while maintaining competitive performance when applied to attention mechanisms in modern LLMs. In particular, our experiments on 1–1.5B parameter models demonstrate that rotor-based modules can effectively reproduce the behavior of dense linear layers when trained in isolation, while our end-to-end experiment on FMNIST shows their feasibility when trained jointly with the rest of the network from scratch. The underlying algebraic structure reveals a rich compositional hierarchy, where geometric primitives combine through rotor operations to form expressive yet compact transformations. This is achieved by mapping bivector parameters to their corresponding rotor operations. These insights open several promising directions, including the development of interpretable architectures and parameter-efficient models that leverage this compositional structure. Beyond that, our framework connects to statistical models involving interaction decomposition, such as ANOVA [St et al., 1989], multivariate analysis [Mardia et al., 2024], and mechanisms to approximate Shapley features [Chen et al., 2023]. For example, modeling high-order dependencies in statistical learning often suffers from exponential parameter growth. While ideas such as Tucker tensor decomposition [Li et al., 2018] factorize the full coefficient tensor, our framework offers an alternative by mapping k predictor variables to a multivector X and modeling the response variable via a rotor transformation as $\hat{y} = \langle \exp(a)X \exp(b)^\dagger \rangle_0$ learned from $\mathcal{O}(k^2)$, where (a, b) are learned bivectors from our algorithms. This constructs interaction spaces through the composition of 2-way primitives.

Practical considerations. Our current implementation remains computationally demanding, since it does not yet exploit the inherent sparsity or algebraic structure of rotor decompositions (see Appendix A for a discussion of limitations). In parallel, a promising direction is to leverage these ideas to mitigate memory bandwidth bottlenecks that dominate large-model inference. As noted in Davies et al. [2025], (i) memory capacity requirements for frontier LLMs exceed hundreds of gigabytes, and (ii) memory bandwidth, rather than compute, is the primary bottleneck for inference throughput. Our approach directly addresses (ii): instead of loading millions of dense-layer weights from memory, rotor layers can, in principle, synthesize them on-chip from a small set of geometric parameters, effectively trading compute for memory bandwidth. Future work will focus on developing sparse and hardware-aware Clifford kernels to realize these gains in practice and on extending the framework to full-model training and dynamic rotor composition for scalable deployment.

Acknowledgments

We thank the anonymous reviewers for their constructive feedback. We are very grateful to Prof. Karthikeyan Sankaralingam for numerous valuable discussions and working out the link to Davies et al. [2025]. TP, DY and VS were all partly supported by NIH R01AG092220.

References

Samira Abnar, Omid Saremi, Laurent Dinh, Shantel Wilson, Miguel Angel Bautista, Chen Huang, Vimal Thilak, Eta Littwin, Jiatao Gu, Josh Susskind, and Samy Bengio. Adaptivity and modularity for efficient generalization over task complexity, 2023. URL <https://arxiv.org/abs/2310.08866>.

Mohammad Mahmudul Alam, Alexander Oberle, Edward Raff, Stella Biderman, Tim Oates, and James Holt. A walsh hadamard derived linear vector symbolic architecture. *arXiv preprint arXiv:2410.22669*, 2024.

Francesco Alesiani. Pytorch geometric algebra. URL https://github.com/falesiani/torch_ga.

Shaojie Bai, J. Zico Kolter, and Vladlen Koltun. Deep equilibrium models, 2019. URL <https://arxiv.org/abs/1909.01377>.

Johannes Brandstetter, Rianne van den Berg, Max Welling, and Jayesh K. Gupta. Clifford neural layers for pde modeling, 2023. URL <https://arxiv.org/abs/2209.04934>.

Julian Büchel, Athanasios Vasilopoulos, William Andrew Simon, Irem Boybat, HsinYu Tsai, Geofrey W Burr, Hernan Castro, Bill Filipiak, Manuel Le Gallo, Abbas Rahimi, et al. Efficient scaling of large language models with mixture of experts and 3d analog in-memory computing. *Nature Computational Science*, pages 1–14, 2025.

Hui Chen, Viet Luong, Lopamudra Mukherjee, and Vikas Singh. Simpletm: A simple baseline for multivariate time series forecasting. In *The Thirteenth International Conference on Learning Representations*, 2025.

Lu Chen, Siyu Lou, Keyan Zhang, Jin Huang, and Quanshi Zhang. Harsanyinet: Computing accurate shapley values in a single forward propagation. *arXiv preprint arXiv:2304.01811*, 2023.

Xinyun Chen, Chen Liang, Adams Wei Yu, Dawn Song, and Denny Zhou. Compositional generalization via neural-symbolic stack machines. *Advances in Neural Information Processing Systems*, 33: 1690–1701, 2020.

Yu Cheng, Felix X Yu, Rogerio S Feris, Sanjiv Kumar, Alok Choudhary, and Shi-Fu Chang. An exploration of parameter redundancy in deep networks with circulant projections. In *Proceedings of the IEEE international conference on computer vision*, pages 2857–2865, 2015.

Sotirios Panagiotis Chytas, Hyunwoo J Kim, and Vikas Singh. Understanding multi-compositional learning in vision and language models via category theory. In *European Conference on Computer Vision*, pages 324–341. Springer, 2024.

Peter Clark, Isaac Cowhey, Oren Etzioni, Tushar Khot, Ashish Sabharwal, Carissa Schoenick, and Oyvind Tafjord. Think you have solved question answering? try arc, the ai2 reasoning challenge, 2018. URL <https://arxiv.org/abs/1803.05457>.

P. M. Cohn. *Basic Algebra: Groups, Rings and Fields*. Springer, London, 2003. doi: 10.1007/978-0-85729-428-9.

Keith Conrad. Exterior powers. Lecture notes, Department of Mathematics, University of Connecticut, n.d. Available at <https://kconrad.math.uconn.edu/blurbs/linmultialg/extmod.pdf>.

Abhishek Das, Georgia Gkioxari, Stefan Lee, Devi Parikh, and Dhruv Batra. Neural modular control for embodied question answering. In *Conference on robot learning*, pages 53–62. PMLR, 2018.

Michael Davies, Neal Crago, Karthikeyan Sankaralingam, and Christos Kozyrakis. Efficient llm inference: Bandwidth, compute, synchronization, and capacity are all you need, 2025. URL <https://arxiv.org/abs/2507.14397>.

Jesse Dodge, Maarten Sap, Ana Marasović, William Agnew, Gabriel Ilharco, Dirk Groeneveld, Margaret Mitchell, and Matt Gardner. Documenting large webtext corpora: A case study on the colossal clean crawled corpus, 2021. URL <https://arxiv.org/abs/2104.08758>.

Chris Doran and Anthony Lasenby. *Geometric algebra for physicists*. Cambridge University Press, 2003.

David Eelbode, Martin Roelfs, and Steven De Keninck. Outer and eigen: Tangent concepts, 2024. URL <https://arxiv.org/abs/2412.20566>.

Elias Frantar, Saleh Ashkboos, Torsten Hoefer, and Dan Alistarh. Gptq: Accurate post-training quantization for generative pre-trained transformers. *arXiv preprint arXiv:2210.17323*, 2022.

JEAN QUAINTANCE Gallier and Jocelyn Quaintance. *Differential geometry and lie groups*, volume 12. Springer, 2020.

Badih Ghazi, Rina Panigrahy, and Joshua Wang. Recursive sketches for modular deep learning. In Kamalika Chaudhuri and Ruslan Salakhutdinov, editors, *Proceedings of the 36th International Conference on Machine Learning*, volume 97 of *Proceedings of Machine Learning Research*, pages 2211–2220. PMLR, 09–15 Jun 2019. URL <https://proceedings.mlr.press/v97/ghazi19a.html>.

Herbert Goldstein, Charles P. Poole, and John L. Safko. *Classical Mechanics*. Addison-Wesley, 3rd edition, 2002. ISBN 978-0201657029.

Gene H. Golub and Charles F. Van Loan. *Matrix Computations*. Johns Hopkins University Press, Baltimore, MD, 4th edition, 2013. ISBN 9781421407944.

David Hestenes and Garret Sobczyk. *Clifford algebra to geometric calculus: a unified language for mathematics and physics*, volume 5. Springer Science & Business Media, 2012.

Eckhard Hitzer. Introduction to clifford’s geometric algebra. *arXiv preprint arXiv:1306.1660*, 2013. URL <https://arxiv.org/abs/1306.1660>.

Edward J. Hu, Yelong Shen, Phillip Wallis, Zeyuan Allen-Zhu, Yuanzhi Li, Shean Wang, Lu Wang, and Weizhu Chen. Lora: Low-rank adaptation of large language models, 2021. URL <https://arxiv.org/abs/2106.09685>.

Zijian Hu, Jipeng Zhang, Rui Pan, Zhaozhuo Xu, Shanshan Han, Han Jin, Alay Dilipbhai Shah, Dimitris Stripelis, Yuhang Yao, Salman Avestimehr, Tong Zhang, and Chaoyang He. Fox-1: Open small language model for cloud and edge, 2025. URL <https://arxiv.org/abs/2411.05281>.

Tosio Kato. *Perturbation Theory for Linear Operators*, volume 132 of *Grundlehren der mathematischen Wissenschaften*. Springer-Verlag, Berlin, Heidelberg, 2nd edition, 1980. ISBN 3-540-07558-5. URL <https://webhomes.maths.ed.ac.uk/~v1ranick/papers/kato1.pdf>.

Diederik P. Kingma and Jimmy Ba. Adam: A method for stochastic optimization, 2017. URL <https://arxiv.org/abs/1412.6980>.

Leo Kozachkov, Ksenia V. Kastanenka, and Dmitry Krotov. Building transformers from neurons and astrocytes. *Proceedings of the National Academy of Sciences*, 120(34):e2219150120, 2023. doi: 10.1073/pnas.2219150120. URL <https://www.pnas.org/doi/abs/10.1073/pnas.2219150120>.

Zorah Lähner and Michael Moeller. On the direct alignment of latent spaces. In *Proceedings of UniReps: the First Workshop on Unifying Representations in Neural Models*, pages 158–169. PMLR, 2024.

Brenden Lake and Marco Baroni. Generalization without systematicity: On the compositional skills of sequence-to-sequence recurrent networks. In *International conference on machine learning*, pages 2873–2882. PMLR, 2018.

Mario Lezcano-Casado and David Martínez-Rubio. Cheap orthogonal constraints in neural networks: A simple parametrization of the orthogonal and unitary group, 2019. URL <https://arxiv.org/abs/1901.08428>.

Qing Li, Yixin Zhu, Yitao Liang, Ying Nian Wu, Song-Chun Zhu, and Siyuan Huang. Neural-symbolic recursive machine for systematic generalization. *arXiv preprint arXiv:2210.01603*, 2022.

Xiaoshan Li, Da Xu, Hua Zhou, and Lexin Li. Tucker tensor regression and neuroimaging analysis. *Statistics in Biosciences*, 10(3):520–545, 2018.

Mitch Marcus, Beatrice Santorini, and Mary Ann Marcinkiewicz. Building a large annotated corpus of english: The penn treebank. *Computational linguistics*, 19(2):313–330, 1993.

Kanti V Mardia, John T Kent, and Charles C Taylor. *Multivariate analysis*. John Wiley & Sons, 2024.

Saeed Masoudnia and Reza Ebrahimpour. Mixture of experts: a literature survey. *Artificial Intelligence Review*, 42:275–293, 2014.

Jeff Mitchell and Mirella Lapata. Vector-based models of semantic composition. In *proceedings of ACL-08: HLT*, pages 236–244, 2008.

Jonas Pfeiffer, Sebastian Ruder, Ivan Vulić, and Edoardo Maria Ponti. Modular deep learning. *arXiv preprint arXiv:2302.11529*, 2023.

Mert Pilanci. From complexity to clarity: Analytical expressions of deep neural network weights via clifford’s geometric algebra and convexity, 2024. URL <https://arxiv.org/abs/2309.16512>.

Ofir Press, Muru Zhang, Sewon Min, Ludwig Schmidt, Noah A. Smith, and Mike Lewis. Measuring and narrowing the compositionality gap in language models, 2023. URL <https://arxiv.org/abs/2210.03350>.

Qwen, :, An Yang, Baosong Yang, Beichen Zhang, Binyuan Hui, Bo Zheng, Bowen Yu, Chengyuan Li, Dayiheng Liu, Fei Huang, Haoran Wei, Huan Lin, Jian Yang, Jianhong Tu, Jianwei Zhang, Jianxin Yang, Jiaxi Yang, Jingren Zhou, Junyang Lin, Kai Dang, Keming Lu, Keqin Bao, Kexin Yang, Le Yu, Mei Li, Mingfeng Xue, Pei Zhang, Qin Zhu, Rui Men, Runji Lin, Tianhao Li, Tianyi Tang, Tingyu Xia, Xingzhang Ren, Xuancheng Ren, Yang Fan, Yang Su, Yichang Zhang, Yu Wan, Yuqiong Liu, Zeyu Cui, Zhenru Zhang, and Zihan Qiu. Qwen2.5 technical report, 2025. URL <https://arxiv.org/abs/2412.15115>.

Daking Rai, Yilun Zhou, Shi Feng, Abulhair Saparov, and Ziyu Yao. A practical review of mechanistic interpretability for transformer-based language models. *arXiv preprint arXiv:2407.02646*, 2024.

Carlos Riquelme, Joan Puigcerver, Basil Mustafa, Maxim Neumann, Rodolphe Jenatton, André Susano Pinto, Daniel Keysers, and Neil Houlsby. Scaling vision with sparse mixture of experts. *Advances in Neural Information Processing Systems*, 34:8583–8595, 2021.

Martin Roelfs and Steven De Keninck. Graded symmetry groups: Plane and simple, 2021. URL <https://arxiv.org/abs/2107.03771>.

David Ruhe, Johannes Brandstetter, and Patrick Forré. Clifford group equivariant neural networks, 2023a. URL <https://arxiv.org/abs/2305.11141>.

David Ruhe, Jayesh K. Gupta, Steven de Keninck, Max Welling, and Johannes Brandstetter. Geometric clifford algebra networks, 2023b. URL <https://arxiv.org/abs/2302.06594>.

Sara Sabour, Nicholas Frosst, and Geoffrey E Hinton. Dynamic routing between capsules, 2017. URL <https://arxiv.org/abs/1710.09829>.

Simon Schug, Seijin Kobayashi, Yassir Akram, Maciej Wołczyk, Alexandra Proca, Johannes von Oswald, Razvan Pascanu, João Sacramento, and Angelika Steger. Discovering modular solutions that generalize compositionally, 2024. URL <https://arxiv.org/abs/2312.15001>.

Vikas Sindhwani, Tara Sainath, and Sanjiv Kumar. Structured transforms for small-footprint deep learning. *Advances in Neural Information Processing Systems*, 28, 2015.

Lars St, Svante Wold, et al. Analysis of variance (anova). *Chemometrics and intelligent laboratory systems*, 6(4):259–272, 1989.

Kai Sheng Tai, Richard Socher, and Christopher D Manning. Improved semantic representations from tree-structured long short-term memory networks. *arXiv preprint arXiv:1503.00075*, 2015.

Hugo Touvron, Thibaut Lavril, Gautier Izacard, Xavier Martinet, Marie-Anne Lachaux, Timothée Lacroix, Baptiste Rozière, Naman Goyal, Eric Hambro, Faisal Azhar, Aurelien Rodriguez, Armand Joulin, Edouard Grave, and Guillaume Lample. Llama: Open and efficient foundation language models, 2023. URL <https://arxiv.org/abs/2302.13971>.

Yifei Wang, Sungyoon Kim, Paul Chu, Indu Subramaniam, and Mert Pilanci. Randomized geometric algebra methods for convex neural networks, 2024. URL <https://arxiv.org/abs/2406.02806>.

Gail Weiss, Yoav Goldberg, and Eran Yahav. Thinking like transformers, 2021. URL <https://arxiv.org/abs/2106.06981>.

James H. Wilkinson. *The Algebraic Eigenvalue Problem*. Oxford University Press, Oxford, 1965. URL <https://doi.org/10.1017/S0013091500012104>.

Han Xiao, Kashif Rasul, and Roland Vollgraf. Fashion-mnist: a novel image dataset for benchmarking machine learning algorithms, 2017. URL <https://arxiv.org/abs/1708.07747>.

Chenxi Yang and Swarat Chaudhuri. Safe neurosymbolic learning with differentiable symbolic execution, 2022. URL <https://arxiv.org/abs/2203.07671>.

Felix Yu, Sanjiv Kumar, Yunchao Gong, and Shih-Fu Chang. Circulant binary embedding. In *International conference on machine learning*, pages 946–954. PMLR, 2014.

Rowan Zellers, Ari Holtzman, Yonatan Bisk, Ali Farhadi, and Yejin Choi. Hellaswag: Can a machine really finish your sentence?, 2019. URL <https://arxiv.org/abs/1905.07830>.

Zhanpeng Zeng, Michael Davies, Pranav Pulijala, Karthikeyan Sankaralingam, and Vikas Singh. Lookupffn: making transformers compute-lite for cpu inference. In *International Conference on Machine Learning*, pages 40707–40718. PMLR, 2023.

Xiangyu Zhang, Xinyu Zhou, Mengxiao Lin, and Jian Sun. Shufflenet: An extremely efficient convolutional neural network for mobile devices, 2017. URL <https://arxiv.org/abs/1707.01083>.

Yanli Zhou, Reuben Feinman, and Brenden M Lake. Compositional diversity in visual concept learning. *Cognition*, 244:105711, 2024.

Andy Zou, Long Phan, Sarah Chen, James Campbell, Phillip Guo, Richard Ren, Alexander Pan, Xuwang Yin, Mantas Mazeika, Ann-Kathrin Dombrowski, Shashwat Goel, Nathaniel Li, Michael J. Byun, Zifan Wang, Alex Mallen, Steven Basart, Sanmi Koyejo, Dawn Song, Matt Fredrikson, J. Zico Kolter, and Dan Hendrycks. Representation engineering: A top-down approach to ai transparency, 2025. URL <https://arxiv.org/abs/2310.01405>.

NeurIPS Paper Checklist

1. Claims

Question: Do the main claims made in the abstract and introduction accurately reflect the paper's contributions and scope?

Answer: [\[Yes\]](#)

Justification: The main claim made in the abstract is that we can express a linear layer in $\mathcal{O}(\log^2 d)$ parameters with algebraic primitives. The framework is detailed in Sections 3 and 4 with supporting experimental results in Section 5 and Appendix D.

Guidelines:

- The answer NA means that the abstract and introduction do not include the claims made in the paper.
- The abstract and/or introduction should clearly state the claims made, including the contributions made in the paper and important assumptions and limitations. A No or NA answer to this question will not be perceived well by the reviewers.
- The claims made should match theoretical and experimental results, and reflect how much the results can be expected to generalize to other settings.
- It is fine to include aspirational goals as motivation as long as it is clear that these goals are not attained by the paper.

2. Limitations

Question: Does the paper discuss the limitations of the work performed by the authors?

Answer: [\[Yes\]](#)

Justification: The limitations are discussed in Appendix A.

Guidelines:

- The answer NA means that the paper has no limitation while the answer No means that the paper has limitations, but those are not discussed in the paper.
- The authors are encouraged to create a separate "Limitations" section in their paper.
- The paper should point out any strong assumptions and how robust the results are to violations of these assumptions (e.g., independence assumptions, noiseless settings, model well-specification, asymptotic approximations only holding locally). The authors should reflect on how these assumptions might be violated in practice and what the implications would be.
- The authors should reflect on the scope of the claims made, e.g., if the approach was only tested on a few datasets or with a few runs. In general, empirical results often depend on implicit assumptions, which should be articulated.
- The authors should reflect on the factors that influence the performance of the approach. For example, a facial recognition algorithm may perform poorly when image resolution is low or images are taken in low lighting. Or a speech-to-text system might not be used reliably to provide closed captions for online lectures because it fails to handle technical jargon.
- The authors should discuss the computational efficiency of the proposed algorithms and how they scale with dataset size.
- If applicable, the authors should discuss possible limitations of their approach to address problems of privacy and fairness.
- While the authors might fear that complete honesty about limitations might be used by reviewers as grounds for rejection, a worse outcome might be that reviewers discover limitations that aren't acknowledged in the paper. The authors should use their best judgment and recognize that individual actions in favor of transparency play an important role in developing norms that preserve the integrity of the community. Reviewers will be specifically instructed to not penalize honesty concerning limitations.

3. Theory assumptions and proofs

Question: For each theoretical result, does the paper provide the full set of assumptions and a complete (and correct) proof?

Answer: [\[Yes\]](#)

Justification: The proofs of Alg. 1 and 2 are in Appendix B.

Guidelines:

- The answer NA means that the paper does not include theoretical results.
- All the theorems, formulas, and proofs in the paper should be numbered and cross-referenced.
- All assumptions should be clearly stated or referenced in the statement of any theorems.
- The proofs can either appear in the main paper or the supplemental material, but if they appear in the supplemental material, the authors are encouraged to provide a short proof sketch to provide intuition.
- Inversely, any informal proof provided in the core of the paper should be complemented by formal proofs provided in appendix or supplemental material.
- Theorems and Lemmas that the proof relies upon should be properly referenced.

4. Experimental result reproducibility

Question: Does the paper fully disclose all the information needed to reproduce the main experimental results of the paper to the extent that it affects the main claims and/or conclusions of the paper (regardless of whether the code and data are provided or not)?

Answer: [\[Yes\]](#)

Justification: We detail the experimental setup in Section 5 and give hyperparameters and training details in Appendix C.

Guidelines:

- The answer NA means that the paper does not include experiments.
- If the paper includes experiments, a No answer to this question will not be perceived well by the reviewers: Making the paper reproducible is important, regardless of whether the code and data are provided or not.
- If the contribution is a dataset and/or model, the authors should describe the steps taken to make their results reproducible or verifiable.
- Depending on the contribution, reproducibility can be accomplished in various ways. For example, if the contribution is a novel architecture, describing the architecture fully might suffice, or if the contribution is a specific model and empirical evaluation, it may be necessary to either make it possible for others to replicate the model with the same dataset, or provide access to the model. In general, releasing code and data is often one good way to accomplish this, but reproducibility can also be provided via detailed instructions for how to replicate the results, access to a hosted model (e.g., in the case of a large language model), releasing of a model checkpoint, or other means that are appropriate to the research performed.
- While NeurIPS does not require releasing code, the conference does require all submissions to provide some reasonable avenue for reproducibility, which may depend on the nature of the contribution. For example
 - (a) If the contribution is primarily a new algorithm, the paper should make it clear how to reproduce that algorithm.
 - (b) If the contribution is primarily a new model architecture, the paper should describe the architecture clearly and fully.
 - (c) If the contribution is a new model (e.g., a large language model), then there should either be a way to access this model for reproducing the results or a way to reproduce the model (e.g., with an open-source dataset or instructions for how to construct the dataset).
 - (d) We recognize that reproducibility may be tricky in some cases, in which case authors are welcome to describe the particular way they provide for reproducibility. In the case of closed-source models, it may be that access to the model is limited in some way (e.g., to registered users), but it should be possible for other researchers to have some path to reproducing or verifying the results.

5. Open access to data and code

Question: Does the paper provide open access to the data and code, with sufficient instructions to faithfully reproduce the main experimental results, as described in supplemental material?

Answer: **[Yes]**

Justification: We include our codebase and instructions to run the code in supplementary material.

Guidelines:

- The answer NA means that paper does not include experiments requiring code.
- Please see the NeurIPS code and data submission guidelines (<https://nips.cc/public/guides/CodeSubmissionPolicy>) for more details.
- While we encourage the release of code and data, we understand that this might not be possible, so “No” is an acceptable answer. Papers cannot be rejected simply for not including code, unless this is central to the contribution (e.g., for a new open-source benchmark).
- The instructions should contain the exact command and environment needed to run to reproduce the results. See the NeurIPS code and data submission guidelines (<https://nips.cc/public/guides/CodeSubmissionPolicy>) for more details.
- The authors should provide instructions on data access and preparation, including how to access the raw data, preprocessed data, intermediate data, and generated data, etc.
- The authors should provide scripts to reproduce all experimental results for the new proposed method and baselines. If only a subset of experiments are reproducible, they should state which ones are omitted from the script and why.
- At submission time, to preserve anonymity, the authors should release anonymized versions (if applicable).
- Providing as much information as possible in supplemental material (appended to the paper) is recommended, but including URLs to data and code is permitted.

6. Experimental setting/details

Question: Does the paper specify all the training and test details (e.g., data splits, hyperparameters, how they were chosen, type of optimizer, etc.) necessary to understand the results?

Answer: **[Yes]**

Justification: The details are given in Section 5 with hyperparameters and additional details on data splits and experiments given in Appendix C.

Guidelines:

- The answer NA means that the paper does not include experiments.
- The experimental setting should be presented in the core of the paper to a level of detail that is necessary to appreciate the results and make sense of them.
- The full details can be provided either with the code, in appendix, or as supplemental material.

7. Experiment statistical significance

Question: Does the paper report error bars suitably and correctly defined or other appropriate information about the statistical significance of the experiments?

Answer: **[No]**

Justification: Error bars are not reported for accuracy because it would be too computationally expensive. See Appendix C for GPU hours and resources required.

Guidelines:

- The answer NA means that the paper does not include experiments.
- The authors should answer “Yes” if the results are accompanied by error bars, confidence intervals, or statistical significance tests, at least for the experiments that support the main claims of the paper.

- The factors of variability that the error bars are capturing should be clearly stated (for example, train/test split, initialization, random drawing of some parameter, or overall run with given experimental conditions).
- The method for calculating the error bars should be explained (closed form formula, call to a library function, bootstrap, etc.)
- The assumptions made should be given (e.g., Normally distributed errors).
- It should be clear whether the error bar is the standard deviation or the standard error of the mean.
- It is OK to report 1-sigma error bars, but one should state it. The authors should preferably report a 2-sigma error bar than state that they have a 96% CI, if the hypothesis of Normality of errors is not verified.
- For asymmetric distributions, the authors should be careful not to show in tables or figures symmetric error bars that would yield results that are out of range (e.g. negative error rates).
- If error bars are reported in tables or plots, The authors should explain in the text how they were calculated and reference the corresponding figures or tables in the text.

8. Experiments compute resources

Question: For each experiment, does the paper provide sufficient information on the computer resources (type of compute workers, memory, time of execution) needed to reproduce the experiments?

Answer: [\[Yes\]](#)

Justification: See Appendix C for GPU hours and memory requirements.

Guidelines:

- The answer NA means that the paper does not include experiments.
- The paper should indicate the type of compute workers CPU or GPU, internal cluster, or cloud provider, including relevant memory and storage.
- The paper should provide the amount of compute required for each of the individual experimental runs as well as estimate the total compute.
- The paper should disclose whether the full research project required more compute than the experiments reported in the paper (e.g., preliminary or failed experiments that didn't make it into the paper).

9. Code of ethics

Question: Does the research conducted in the paper conform, in every respect, with the NeurIPS Code of Ethics <https://neurips.cc/public/EthicsGuidelines>?

Answer: [\[Yes\]](#)

Justification: This paper conforms, in every respect, with the NeurIPS Code of Ethics.

Guidelines:

- The answer NA means that the authors have not reviewed the NeurIPS Code of Ethics.
- If the authors answer No, they should explain the special circumstances that require a deviation from the Code of Ethics.
- The authors should make sure to preserve anonymity (e.g., if there is a special consideration due to laws or regulations in their jurisdiction).

10. Broader impacts

Question: Does the paper discuss both potential positive societal impacts and negative societal impacts of the work performed?

Answer: [\[NA\]](#)

Justification: This is a technical paper that has no societal impact.

Guidelines:

- The answer NA means that there is no societal impact of the work performed.
- If the authors answer NA or No, they should explain why their work has no societal impact or why the paper does not address societal impact.

- Examples of negative societal impacts include potential malicious or unintended uses (e.g., disinformation, generating fake profiles, surveillance), fairness considerations (e.g., deployment of technologies that could make decisions that unfairly impact specific groups), privacy considerations, and security considerations.
- The conference expects that many papers will be foundational research and not tied to particular applications, let alone deployments. However, if there is a direct path to any negative applications, the authors should point it out. For example, it is legitimate to point out that an improvement in the quality of generative models could be used to generate deepfakes for disinformation. On the other hand, it is not needed to point out that a generic algorithm for optimizing neural networks could enable people to train models that generate Deepfakes faster.
- The authors should consider possible harms that could arise when the technology is being used as intended and functioning correctly, harms that could arise when the technology is being used as intended but gives incorrect results, and harms following from (intentional or unintentional) misuse of the technology.
- If there are negative societal impacts, the authors could also discuss possible mitigation strategies (e.g., gated release of models, providing defenses in addition to attacks, mechanisms for monitoring misuse, mechanisms to monitor how a system learns from feedback over time, improving the efficiency and accessibility of ML).

11. Safeguards

Question: Does the paper describe safeguards that have been put in place for responsible release of data or models that have a high risk for misuse (e.g., pretrained language models, image generators, or scraped datasets)?

Answer: [NA]

Justification: The paper poses no such risk.

Guidelines:

- The answer NA means that the paper poses no such risks.
- Released models that have a high risk for misuse or dual-use should be released with necessary safeguards to allow for controlled use of the model, for example by requiring that users adhere to usage guidelines or restrictions to access the model or implementing safety filters.
- Datasets that have been scraped from the Internet could pose safety risks. The authors should describe how they avoided releasing unsafe images.
- We recognize that providing effective safeguards is challenging, and many papers do not require this, but we encourage authors to take this into account and make a best faith effort.

12. Licenses for existing assets

Question: Are the creators or original owners of assets (e.g., code, data, models), used in the paper, properly credited and are the license and terms of use explicitly mentioned and properly respected?

Answer: [Yes]

Justification: All datasets, models, and pre-existing code bases used are cited.

Guidelines:

- The answer NA means that the paper does not use existing assets.
- The authors should cite the original paper that produced the code package or dataset.
- The authors should state which version of the asset is used and, if possible, include a URL.
- The name of the license (e.g., CC-BY 4.0) should be included for each asset.
- For scraped data from a particular source (e.g., website), the copyright and terms of service of that source should be provided.
- If assets are released, the license, copyright information, and terms of use in the package should be provided. For popular datasets, paperswithcode.com/datasets has curated licenses for some datasets. Their licensing guide can help determine the license of a dataset.

- For existing datasets that are re-packaged, both the original license and the license of the derived asset (if it has changed) should be provided.
- If this information is not available online, the authors are encouraged to reach out to the asset's creators.

13. New assets

Question: Are new assets introduced in the paper well documented and is the documentation provided alongside the assets?

Answer: [NA]

Justification: This paper does not release new assets.

Guidelines:

- The answer NA means that the paper does not release new assets.
- Researchers should communicate the details of the dataset/code/model as part of their submissions via structured templates. This includes details about training, license, limitations, etc.
- The paper should discuss whether and how consent was obtained from people whose asset is used.
- At submission time, remember to anonymize your assets (if applicable). You can either create an anonymized URL or include an anonymized zip file.

14. Crowdsourcing and research with human subjects

Question: For crowdsourcing experiments and research with human subjects, does the paper include the full text of instructions given to participants and screenshots, if applicable, as well as details about compensation (if any)?

Answer: [NA]

Justification: No crowdsourcing or research with human subjects.

Guidelines:

- The answer NA means that the paper does not involve crowdsourcing nor research with human subjects.
- Including this information in the supplemental material is fine, but if the main contribution of the paper involves human subjects, then as much detail as possible should be included in the main paper.
- According to the NeurIPS Code of Ethics, workers involved in data collection, curation, or other labor should be paid at least the minimum wage in the country of the data collector.

15. Institutional review board (IRB) approvals or equivalent for research with human subjects

Question: Does the paper describe potential risks incurred by study participants, whether such risks were disclosed to the subjects, and whether Institutional Review Board (IRB) approvals (or an equivalent approval/review based on the requirements of your country or institution) were obtained?

Answer: [NA]

Justification: No research with human subjects.

Guidelines:

- The answer NA means that the paper does not involve crowdsourcing nor research with human subjects.
- Depending on the country in which research is conducted, IRB approval (or equivalent) may be required for any human subjects research. If you obtained IRB approval, you should clearly state this in the paper.
- We recognize that the procedures for this may vary significantly between institutions and locations, and we expect authors to adhere to the NeurIPS Code of Ethics and the guidelines for their institution.
- For initial submissions, do not include any information that would break anonymity (if applicable), such as the institution conducting the review.

16. Declaration of LLM usage

Question: Does the paper describe the usage of LLMs if it is an important, original, or non-standard component of the core methods in this research? Note that if the LLM is used only for writing, editing, or formatting purposes and does not impact the core methodology, scientific rigorousness, or originality of the research, declaration is not required.

Answer: [NA]

Justification: None used

Guidelines:

- The answer NA means that the core method development in this research does not involve LLMs as any important, original, or non-standard components.
- Please refer to our LLM policy (<https://neurips.cc/Conferences/2025/LLM>) for what should or should not be described.

Appendix

In the Appendix, we provide additional discussions, formal proofs, and further experimental details that support the main paper. Section A outlines the limitations of this work. Section B presents the proofs of the algorithms and theorems, along with general results for certain special cases. Section C describes the hyperparameters and training setups used in the experiments. Section D includes additional experimental results.

A Limitations

While our results demonstrate feasibility, they remain theoretical at this stage—though rotor layers achieve competitive performance when replacing attention layers, the benefits are primarily in a radical parameter count reduction rather than immediate compute speedup in practice. Realizing such gains will require dedicated systems-level optimizations beyond the scope of this work.

Our current implementation relies on dense matrix representations of rotors and does not yet exploit the inherent sparsity of the rotor decomposition. Leveraging this sparsity will require new backpropagation schemes and software libraries, particularly when training from scratch. We discuss the matrix representation and sparse structure of rotors in detail in Section B.

Overall, this work is intended to highlight the feasibility and promise of decomposing linear layers—key building blocks in modern large models—into smaller (potentially geometric) modules, such as bivectors and rotors, to facilitate more compact and interpretable architectures.

B Proofs

B.1 Correctness Proofs for Main Algorithms

We prove the correctness of Alg. 1 and 2 in the theorems below.

Theorem 2. *Given a bivector $b \in \text{Cl}^2(n)$, a random vector $v \in \text{Cl}^1(n)$ that has a non-zero component in the direction of the dominant simple component, and a threshold $\epsilon \in \mathbb{R}$, Alg. 2 returns an approximate simple projection of b in a differentiable way.*

Proof. Let $B \in \mathfrak{so}(n)$ be the skew-symmetric matrix corresponding to b . We begin by showing that $b \lrcorner v = Bv$ for any vector v . Fix an orthonormal basis $\{e_1, \dots, e_n\}$ of \mathbb{R}^n and let

$$b = \sum_{1 \leq i < j \leq n} b_{ij} (e_i \wedge e_j) \quad \text{and} \quad v = \sum_{k=1}^n v_k e_k,$$

noting that $[B]_{ij} = b_{ij}$ for $1 \leq i < j \leq n$ and $[B]_{ij} = -b_{ji}$ for $1 \leq j < i \leq n$. It is easy to verify that $(e_i \wedge e_j) \lrcorner v = v_j e_i - v_i e_j$. By bilinearity of the right contraction, we have

$$\begin{aligned} b \lrcorner v &= \sum_{i < j} b_{ij} (v_j e_i - v_i e_j) \\ &= \sum_{i < j} b_{ij} (v_j e_i) - \sum_{i < j} b_{ij} (v_i e_j) \\ &= \sum_{i < j} b_{ij} (v_j e_i) - \sum_{j < i} b_{ji} (v_j e_i) \quad \text{swapping } i \text{ and } j \\ &= \sum_{i < j} [B]_{ij} (v_j e_i) + \sum_{j < i} [B]_{ij} (v_j e_i) \\ &= \sum_i \sum_j [B]_{ij} v_j e_i = \sum_i (Bv)_i e_i = Bv. \end{aligned}$$

It follows that

$$b \lrcorner (b \lrcorner v) = b \lrcorner Bv = B^2 v = -B^T B v.$$

Since B^2 is symmetric, we may apply the power iteration method. Observe, by skew-symmetry, the non-zero eigenvalues of B come in conjugate pairs

$$\{\pm i\sigma_1, \pm i\sigma_2, \dots, \pm i\sigma_k\},$$

with $\sigma_1 \geq \sigma_2 \geq \dots \geq \sigma_k$ and $k \leq \lfloor n/2 \rfloor$. An associated orthonormal set of complex eigenvectors can be written as $\{u_j \pm iv_j\}_{j \leq k}$. Since σ_1 , the dominant eigenvalue for B^2 , has multiplicity 2, the power method on B^2 will not converge in a single direction. Instead, it will *oscillate* within the two-dimensional span of $\{u_1, v_1\}$ Wilkinson [1965].

Let v be one of the singular vectors on which the algorithm terminates. Since singular vectors are unique up to rotation, WLOG we choose v to be the right singular vector. Then, the left singular vector u and singular value σ satisfy $b \llcorner v = Bv = \sigma u$ by definition.

By the Eckart-Young-Mirsky theorem [Golub and Van Loan, 2013], the best rank-2 approximation to B is its projection onto its simple two-dimensional subspace spanned by top two singular directions:

$$\text{Proj}_{\text{simple}}(b) = \sigma_1 u_1 v_1^T + \sigma_2 u_2 v_2^T.$$

As the singular values come in pairs for B , this reduces to $\sigma_1 (u_1 v_1^T + u_2 v_2^T)$. But for B , the two right singular vectors v_1, v_2 and the two left singular vectors u_1, u_2 lie in the same two-plane, coming from the dominant eigenvalue conjugate pair, $\pm i\sigma_1$. Thus, we can choose $u_2 = v_1$ and $v_2 = -u_1$ (or vice versa), which ensures $u_1 \perp v_1$ and $u_2 \perp v_2$. It follows that

$$\text{Proj}_{\text{simple}}(b) = \sigma_1 (u_1 v_1^T - v_1 u_1^T) = \sigma_1 (u_1 \wedge v_1).$$

Since Alg 2 solves only approximately for $\sigma(u \wedge v) \approx \sigma_1(u_1 \wedge v_1)$, we have that

$$\text{Proj}_{\text{simple}}(b) \approx \sigma_1(u_1 \wedge v_1).$$

Note that since the right contraction implementation is differentiable, Alg 2 is differentiable. \square

Theorem 3. *Given $b \in \text{Cl}^2(n)$ and $k - 1$ many vectors $v \in \text{Cl}^1(n)$, Alg. 1 returns the invariant decomposition in a differentiable way.*

Proof. The heavy lifting is done by Eelbode et al. [2024] in Lem. 2, which states that b can be written as the sum of at most k commuting, orthogonal, simple bivectors

$$b = \sum_{j=1}^k \mu_j \frac{v_{\mu_j^+} \wedge v_{\mu_j^-}}{v_{\mu_j^+} \cdot v_{\mu_j^-}}$$

where $\{\pm\mu_1, \pm\mu_2, \dots, \pm\mu_k\}$ is the spectrum of b and $v_{\mu_j^+}$ and $v_{\mu_j^-}$ are partner eigenvectors.

To obtain the full decomposition, it suffices to iteratively extract each term. If we have a differentiable subroutine to find the first term, then we can subtract it from b , apply the same routine to the residual, and repeat. Thus, it suffices to prove that the first term in the sum is equal to the projection of b onto the simple bivectors.

From the proof of Alg. 2, we know that

$$\text{Proj}_{\text{simple}}(b) = \sigma(u \wedge v)$$

where σ is the largest singular value and u, v are the corresponding left and right singular vectors. We wish to show that

$$\sigma(u \wedge v) = \mu_1 \frac{v_{\mu_1^+} \wedge v_{\mu_1^-}}{v_{\mu_1^+} \cdot v_{\mu_1^-}}.$$

The partner eigenvectors take the form $v_{\mu_1^+} = u + iv$ and $v_{\mu_1^-} = u - iv$, as cited in the proof of Alg. 2. Then, the numerator reduces to

$$\begin{aligned} v_{\mu_1^+} \wedge v_{\mu_1^-} &= (u + iv) \wedge (u - iv) \\ &= u \wedge u - iu \wedge v + iv \wedge u + v \wedge u \\ &= -iu \wedge v + iv \wedge u \\ &= -2iu \wedge v. \end{aligned}$$

as the wedge product is antisymmetric. The denominator reduces to

$$\begin{aligned} v_{\mu_1^+} \cdot v_{\mu_1^-} &= (u + iv) \cdot (u - iv) \\ &= u \cdot u - iu \cdot v + iv \cdot u + v \cdot v \\ &= u \cdot u + v \cdot v \\ &= 2 \end{aligned}$$

as singular vectors are orthonormal. Since $\mu_1 = i\sigma$, we have that

$$\mu_1 \frac{v_{\mu_1^+} \wedge v_{\mu_1^-}}{v_{\mu_1^+} \cdot v_{\mu_1^-}} = i\sigma \frac{-2iu \wedge v}{2} = \sigma(u \wedge v) = \text{Proj}_{\text{simple}}(b),$$

as desired. Subtraction is differentiable and as $\text{Proj}_{\text{simple}}(b)$ can be found in a differentiable way, this algorithm is differentiable. \square

B.2 Parameter Count

We revisit the main theorem on the parameter count for rotor maps and provide a proof of the statement.

Theorem 4 (ψ Parameter Count). *Let $\psi : \mathbb{R}^{d_{in}} \rightarrow \mathbb{R}^{d_{out}}$ be a linear map composed of rotor modules $\psi_{r_{ij}, s_{ij}}$ with $i \in [c_1]$ and $j \in [c_2]$, each acting in $\text{Cl}(n)$. Let $2^n \leq d \triangleq \min(d_{in}, d_{out})$. Then, the total number of learnable parameters is upper bounded by*

$$2c_1c_2 \binom{n}{2} = \mathcal{O}(\log^2 d).$$

Proof. Each rotor is the exponential of a bivector. As general bivectors are a linear combination of basis bivectors, of which there are $\binom{n}{2}$, parametrizing a bivector takes $\binom{n}{2}$ scalar parameters. Hence, a single rotor-sandwich map $\psi_{r_{ij}, s_{ij}}$ is parametrized using $2\binom{n}{2}$ scalar parameters. The result is then immediate, since there are c_1c_2 such modules, corresponding to all input and output pairs. \square

Tab. 7 summarizes the number of parameters required for each key, query, and value projection per attention layer using different replacement methods across all LLMs used in our experiments.

B.3 Technical Analysis of Matrix Representation of Rotor Application

We implement the sandwich product in (2), along with other operations such as grade-restricted wedge and inner products, using the `torch_ga` Clifford algebra package for PyTorch, available at Alesiani. In our implementation of (2), the rotor action is represented by a matrix M . In this section, we describe the construction of M and introduce some of its key properties. These results highlight the special orthogonality and block structure of M . While the two-rotor map $\psi_{r,s}(x)$ in (6) does not satisfy these properties exactly, it appears to share similar properties and structure; we do not discuss it here.

We compute the sandwich product using a change-of-basis matrix.

Definition 2. *Let $r \in \text{Spin}(n)$, and let $\{e_J\}_{J \subseteq [n]}$ denote the canonical basis of $\text{Cl}(n)$ (where J is an ordered multi-index). Define*

$$N_r = [\tau(\psi_r(e_J))]_{J \subseteq [n]},$$

where $\psi_r(x) = rxr^\dagger$ and τ is the canonical vector-space isomorphism $\tau : \text{Cl}(n) \rightarrow \mathbb{R}^{2^n}$. That is, each row of N_r is the coefficients of re_Jr^\dagger expressed in the basis. We refer to N_r as the change-of-basis matrix for r .

Lemma 3. *Let $x \in \text{Cl}(n)$, $r \in \text{Spin}(n)$, and N_r be defined as in Def. 2. Then, the two mappings*

$$x \mapsto xN_r \quad \text{and} \quad x \mapsto rxr^\dagger$$

are the same linear map up to isomorphism.

Proof. Write x as

$$x = \sum_{J \subseteq [n]} x_J e_J,$$

where x_J is the real coefficient of the basis element e_J . Let $\tau : \text{Cl}(n) \rightarrow \mathbb{R}^{2^n}$ be the canonical vector-space isomorphism that gives the row vector coordinates of the multivector, $\phi_r(x) = rxr^\dagger$ for $x \in \text{Cl}(n)$, and $\delta(y) = yN_r$ for $y \in \mathbb{R}^{2^n}$. To prove ϕ and δ are the same up to isomorphism, we must prove that $\tau(\phi_r(x)) = \delta(\tau(x))$ for all $x \in \text{Cl}(n)$.

For each basis element e_J , the sandwich product gives some multivector $\psi(e_J) = re_Jr^\dagger$, which we express as

$$re_Jr^\dagger = \sum_{I \subseteq [n]} [N_r]_{J,I} e_I,$$

since $(N_r)_{J,I}$ stores the coefficient of e_I in re_Jr^\dagger by definition. Then,

$$\begin{aligned} \tau(\phi_r(x)) &= \tau(rx r^\dagger) \\ &= \tau\left(r\left[\sum_{J \subseteq [n]} x_J e_J\right] r^\dagger\right) \\ &= \tau\left(\sum_{J \subseteq [n]} x_J r e_J r^\dagger\right) \\ &= \tau\left(\sum_{J \subseteq [n]} x_J \left[\sum_{I \subseteq [n]} [N_r]_{J,I} e_I\right]\right) \\ &= \tau\left(\sum_{I \subseteq [n]} \left[\sum_{J \subseteq [n]} x_J [N_r]_{J,I}\right] e_I\right) \\ &= \sum_{I \subseteq [n]} \left[\sum_{J \subseteq [n]} x_J [N_r]_{J,I}\right] \tau(e_I) \quad \text{by linearity} \\ &= \tau(x) N_r \\ &= \delta(\tau(x)) \end{aligned}$$

where the second to last step follows as the inner sum is the dot product of $\tau(x)$ with the I th column of N_r . \square

This allows us to compute the rotor sandwich product via matrix multiplication. However, this gives us very little insight into the structure of N_r itself. For one, N_r must respect the grade-preserving property of rotors, meaning it is a block diagonal matrix. The following alternative view provides more insight into its structure.

A more revealing view of N_r . Let $b \in \text{Cl}^2(n)$ be the bivector associated with $r \in \text{Spin}(n)$ by $r = \exp(b)$, and let $B \in \mathfrak{so}(n)$ be the corresponding skew-symmetric matrix. Let $R \triangleq \exp(2B) \in \text{SO}(n)$ via the matrix exponential map. For each grade $0 \leq k \leq n$, set

$$M_k \triangleq C_k(R) \in \mathbb{R}^{\binom{n}{k} \times \binom{n}{k}},$$

where $C_k(R)$ is the k th compound matrix of R . Algebraically, $C_k(R)$ is the k th exterior power of R , i.e., the unique linear map $\bigwedge^k(R)$ such that

$$\bigwedge^k(R)(m_1 \wedge m_2 \wedge \cdots \wedge m_k) = Rm_1 \wedge Rm_2 \wedge \cdots \wedge Rm_k$$

for all $m_i \in \mathbb{R}^n$ for $i \in [k]$ [Conrad, n.d.].

Definition 3. Let M_k be the k th compound, or exterior power, of R . Stack the M_k on the diagonal to form

$$M \triangleq \text{diag}(M_0, M_1, \dots, M_n) \in \mathbb{R}^{2^n \times 2^n}.$$

We first show that N_r and M are in fact the same matrix.

Theorem 5. Let N_r and M be defined as in Def. 2 and 3. Then, $M = N_r$.

Proof. The rotor sandwich product is a grade-preserving automorphism, implying $\psi_r(\text{Cl}^k(n)) = \text{Cl}^k(n)$. Thus, N_r is block-diagonal, one block per grade. First, we show $\psi_r(v) = Rv$ for a vector v , where $R = \exp(2B)$. Observe

$$rvr^\dagger = e^b v (e^b)^\dagger = e^b v e^{b^\dagger} = e^b v e^{-b},$$

where the second equality follows as reversion is an anti-automorphism and the third equality follows as $b^\dagger = -b$. Now, consider the adjoint operator in an associative algebra defined as $\text{ad}_X(Y) \triangleq [X, Y] = XY - YX$. The Hadamard lemma and Taylor expansion together imply

$$e^b v e^{-b} = \sum_{k \geq 0} \frac{1}{k!} (\text{ad}_b)^k(v) = \exp(\text{ad}_b)v.$$

We also note the following identity:

$$\text{ad}_b(v) = bv - vb = (b \cdot v + b \wedge v) - (v \cdot b + v \wedge b) = 2b \cdot v = 2Bv,$$

where B is the skew-symmetric matrix for b . Putting these together, it follows that $\psi_r(v) \triangleq rvr^\dagger = \exp(2B)v = Rv$. Now, consider any k -vector $v = e_{i_1} \wedge \cdots \wedge e_{i_k}$. We have

$$\begin{aligned} \psi_r(v) &= \psi(e_{i_1}) \wedge \cdots \wedge \psi(e_{i_k}) & \psi_r \text{ is a grade-preserving automorphism} \\ &= (Re_{i_1}) \wedge \cdots \wedge (Re_{i_k}) & \text{from above} \\ &= \bigwedge^k (R)(v). \end{aligned}$$

Since the mapping is unique, we are done. \square

Note that this block-diagonal structure highlights the *grade-preserving behavior of rotors*. This motivates our design choice to allow grade-mixing in our gadget for more expressivity. In particular, we insert random permutations between rotor layers so that information can mix across different grade components of the input multivector. Now that we have an alternative characterization of the sandwich product, we analyze its structure and the space in which it lives. Below, we examine several structural properties of the matrix M .

Property 1. *The matrix M in Def. 3 is a block diagonal matrix with at most $\binom{2n}{n}$ non-zero entries.*

Proof. $M = N_r$ by Thm. 5 and so M is block diagonal. There are $n + 1$ blocks, each of size $\binom{n}{k} \times \binom{n}{k}$ for $0 \leq k \leq n$. Thus, the total number of non-zero entries is at most

$$\sum_{k=0}^n \binom{n}{k}^2 = \binom{2n}{n},$$

which is far less than the 2^{2n} of a dense $2^n \times 2^n$ matrix. \square

Property 2. *For every grade $0 \leq k \leq n$, the block $M_k = C_k(R)$ lies in $\text{SO}(\binom{n}{k})$. Consequently, $M \in \text{SO}(2^n)$.*

Proof. By assumption, $B \in \mathfrak{so}(n)$, and so $\exp(2B) = R \in \text{SO}(n)$. Taking the k th exterior power preserves orthogonality and a determinant of 1. For each k , the k th compound matrix $M_k = C_k(R)$ is the matrix representation of the k th exterior power $\bigwedge^k (R)$ with respect to the standard basis of k -vectors. Since R is orthogonal, $\bigwedge^k (R)$ preserves the induced inner product on k -vectors, making M_k orthogonal. Moreover, since $\det(R) = 1$, we have $\det(M_k) = \det(\bigwedge^k (R)) = (\det(R))^{\binom{n-1}{k-1}} = 1$.

Therefore, $M_k \in \text{SO}(\binom{n}{k})$ for all $0 \leq k \leq n$. To prove $M \in \text{SO}(2^n)$, we note that since M is block diagonal, $M^T = \text{diag}(M_0^T, \dots, M_n^T)$ and so $M^T M = I$ as the M_k are special orthogonal. $\det(M) = 1$ as the determinant of block diagonal matrices is the product of the determinant of the blocks, meaning $\det(M) = \prod_{k=0}^n \det(M_k) = \prod_{k=0}^n 1 = 1$. \square

Note that under this view, we obtain a map from $\mathfrak{so}(n)$ to $\mathrm{SO}(2^n)$ by first applying the surjective exponential map from $\mathfrak{so}(n)$ to $\mathrm{SO}(n)$, and then lifting $\mathrm{SO}(n)$ to $\mathrm{SO}(2^n)$ via the exterior powers. This transformation enables an *exponential reduction in the number of parameters required to represent rotor layers*. We conclude by identifying the class of matrices which M belongs. The following is a simple but useful characterization. The group of invertible elements of $\mathrm{Cl}(n)$ is

$$\mathrm{Cl}^\times(n) = \{a \in \mathrm{Cl}(n) \mid \exists a^{-1} \in \mathrm{Cl}(n) \text{ st. } aa^{-1} = a^{-1}a = 1\}.$$

Let

$$\phi : \mathrm{Cl}^\times(n) \rightarrow \mathrm{GL}(2^n, \mathbb{R})$$

be the mapping which assigns to each $a \in \mathrm{Cl}^\times(n)$ its change-of-basis matrix N_a . Then for any N_r corresponding to $r \in \mathrm{Spin}(n)$,

$$N_r \in \phi(\mathrm{Spin}(n)).$$

We now give a more refined version of Prop. 2.

Property 3. *Let ϕ be defined as above. Then,*

$$\phi(\mathrm{Spin}(n)) = \mathrm{SO}(2^n) \cap \phi(\mathrm{Cl}^\times(n)).$$

Proof. The first direction, $\phi(\mathrm{Spin}(n)) \subseteq \mathrm{SO}(2^n) \cap \phi(\mathrm{Cl}^\times(n))$, is immediate. If $r \in \mathrm{Spin}(n)$, then by definition r is an invertible element in $\mathrm{Cl}^+(n)$ which satisfies $rr^\dagger = 1_s$ (where 1_s denotes the scalar identity). Thus, $\mathrm{Spin}(n) \subseteq \mathrm{Cl}^\times(n)$, which implies $\phi(\mathrm{Spin}(n)) \subseteq \phi(\mathrm{Cl}^\times(n))$. Furthermore, Prop. 2 and Thm 5 state $N_r \in \mathrm{SO}(2^n)$ for $r \in \mathrm{Spin}(n)$, which ensures $\phi(\mathrm{Spin}(n)) \subseteq \mathrm{SO}(2^n)$.

For the other direction $\mathrm{SO}(2^n) \cap \phi(\mathrm{Cl}^\times(n)) \subseteq \phi(\mathrm{Spin}(n))$, we start by taking an arbitrary element from the set on the LHS and show it must also be in the set on the RHS. Thus, we assume $g \in \mathrm{Cl}^\times(n)$ (an invertible multivector) such that its corresponding matrix $N_g = \phi(g)$ is in $\mathrm{SO}(2^n)$. We wish to show $g \in \mathrm{Spin}(n)$. To do this, it suffices to prove two conditions: $gg^\dagger = 1_s$ (i.e., g is unit-norm), and $g \in \mathrm{Cl}^+(n)$ (i.e., g is an even multivector).

The matrix N_g represents the linear transformation $T_g(X) = gXg^\dagger$. The condition $N_g \in \mathrm{SO}(2^n)$ means that N_g is an orthogonal matrix with $\det(N_g) = 1_s$. We know that due to orthogonality, T_g preserves the canonical inner product on $\mathrm{Cl}(n)$. We define this inner product as $\langle X, Y \rangle = \langle X^\dagger Y \rangle_0$, where $\langle \cdot \rangle_0$ denotes the scalar part of a multivector.

We will first show that $g^\dagger g = 1_s$. Since T_g is an orthogonal transformation w.r.t. $\langle X, Y \rangle = \langle X^\dagger Y \rangle_0$, it must satisfy $T_g^* T_g = \mathrm{I}$, where I is the identity map and T_g^* is the adjoint of T_g w.r.t. the inner product. The adjoint T_g^* is given by $T_g^*(Y) = g^\dagger Y g$. This can be verified by checking the main property of an adjoint, $\langle Y, T_g(X) \rangle = \langle T_g^*(Y), X \rangle$:

$$\begin{aligned} \langle Y, T_g(X) \rangle &= \langle Y^\dagger (gXg^\dagger) \rangle_0 \\ &= \langle (g^\dagger Y^\dagger g) X \rangle_0 \quad (\text{cyclically permute multivectors inside} \\ &\quad \text{scalar part operation, } \langle MNP \rangle_0 = \langle PMN \rangle_0) \\ &= \langle (g^\dagger Y g)^\dagger X \rangle_0 \quad (\text{since } (ABC)^\dagger = C^\dagger B^\dagger A^\dagger \text{ and } (A^\dagger)^\dagger = A) \\ &= \langle T_g^*(Y), X \rangle. \end{aligned}$$

Now, applying the condition $T_g^* T_g = \mathrm{I}$ means $T_g^*(T_g(X)) = X$ for all $X \in \mathrm{Cl}(n)$. Substituting the explicit forms for T_g and T_g^* , we get

$$\begin{aligned} g^\dagger (gXg^\dagger) g &= X \\ (g^\dagger g) X (g^\dagger g) &= X. \end{aligned}$$

Let $A = g^\dagger g$. The equation becomes $AXA = X$ for all $X \in \mathrm{Cl}(n)$. By the Wedderburn-Artin theorem Cohn [2003], the Clifford algebra $\mathrm{Cl}(n, 0)$ is isomorphic to a matrix algebra (or a direct sum of two such algebras) over \mathbb{R} , \mathbb{C} , or \mathbb{H} . In such matrix algebras (and hence in $\mathrm{Cl}(n, 0)$ or its relevant simple components where A lives, noting A is even), if an element A satisfies $AXA = X$ for all elements X of the algebra, then A must be a scalar multiple of the identity, specifically $\pm 1_s$. Therefore, we must have $A = g^\dagger g = \pm 1_s$.

Fix an orthonormal basis e_J (where J is an ordered multi-index). Note that $e_J^\dagger e_J = 1_s$ for every e_J . Write $g = \sum_J c_J e_J$ for scalar coefficients $c_J \in \mathbb{R}$. Then, the scalar part of $g^\dagger g$ is $\langle g^\dagger g \rangle_0 = \sum_J c_J^2$. Since g is invertible, we have $g \neq 0$, so at least one $c_J \neq 0$, making this sum strictly positive. Since $g^\dagger g = \lambda \cdot 1_s$ (where $\lambda = \pm 1_s$), its scalar part is λ . As this scalar part $\langle g^\dagger g \rangle_0$ must be positive, we must conclude that $\lambda = 1_s$, so $g^\dagger g = 1_s$.

Next, we will show that $gg^\dagger = 1_s$. From the previous result, $g^\dagger g = 1_s$. This means g is invertible and its unique inverse is $g^{-1} = g^\dagger$. Then, we can write $gg^\dagger = gg^{-1} = 1_s$. This helps us establish the first condition required for g to be an element of $\text{Spin}(n)$.

Finally, we will need to show that $g \in \text{Cl}^+(n)$ (i.e., g is an even multivector). Since $N_g \in \text{SO}(2^n)$, we have $\det(N_g) = 1_s$. Since $gg^\dagger = 1_s$, it follows that $g^\dagger = g^{-1}$. The transformation can now be written as $T_g(X) = gXg^{-1}$, which is an inner automorphism of $\text{Cl}(n)$ induced by g ; such transformations are algebra automorphisms, meaning that they preserve the algebraic product structure (i.e., $T_g(XY) = T_g(X)T_g(Y)$). The elements g that satisfy $gg^\dagger = 1_s$ are known as versors. Versors who are products of an odd number of vectors (odd versors) are elements of $\text{Pin}(n) \setminus \text{Spin}(n)$, while those that are products of an even number of vectors (even versors) are elements of $\text{Spin}(n)$. Note that $\text{Pin}(n)$ is the group of all such versors, and $\text{Spin}(n) = \text{Pin}(n) \cap \text{Cl}^+(n)$.

We know that if g were indeed an odd versor (an element of $\text{Pin}(n) \setminus \text{Spin}(n)$), the induced inner automorphism $X \mapsto gXg^{-1}$ when restricted to the vector subspace $\text{Cl}^1(n)$ is an orthogonal transformation with determinant -1_s (as it includes a reflection, reversing orientation). It is a known result from the representation theory of Clifford algebras that the determinant of the full automorphism $N_g : X \mapsto gXg^{-1}$ acting on the entire algebra $\text{Cl}(n)$ corresponds to the parity of the versor g . Specifically, $\det(N_g) = +1_s$ if g is an even versor (i.e., $g \in \text{Spin}(n)$), and $\det(N_g) = -1_s$ if g is an odd versor (i.e., $g \in \text{Pin}(n) \setminus \text{Spin}(n)$). This directly links the parity of the versor g to the determinant of the full transformation matrix N_g . Since we know $\det(N_g) = 1_s$, g must be an even versor, i.e., $g \in \text{Cl}^+(n)$.

Since we have shown both $gg^\dagger = 1_s$ and $g \in \text{Cl}^+(n)$, we must conclude that $g \in \text{Spin}(n)$ by its definition. Thus, $\text{SO}(2^n) \cap \phi(\text{Cl}^\times(n)) \subseteq \phi(\text{Spin}(n))$. □

Prop. 3 provides an alternative characterization of the group of matrices associated with rotor conjugation, i.e., N_r lives in the intersection of the special orthogonal group and the subgroup of matrices defined by the group of units of $\text{Cl}(n)$.

C Hyperparameters and Experiment Details

We detail the training configurations for all experiments involving Rotor, Low-Rank (LR), and Block-Hadamard (BH) projections used to approximate attention layers.

C.1 Training Details

Learning approximation layers in attention. To approximate the linear projections in attention layers of an LLM, we train all replacement modules (Rotor, LR, or BH) by minimizing mean squared error (MSE) loss between the predicted and true projection outputs, based on latent representations extracted from LLMs.

Formally, let $W \in \mathbb{R}^{d_{\text{out}} \times d_{\text{in}}}$ be the dense projection matrix (i.e., query, key, or value) we want to approximate within a transformer block. Given hidden input $x \in \mathbb{R}^{d_{\text{in}}}$, the projection computes $y = Wx \in \mathbb{R}^{d_{\text{out}}}$. To train an approximate layer, we collect a dataset $\mathcal{D} = \{(x_i, y_i)\}_{i=1}^N$ by prompting the LLM with a set of prompts $\{P_j\}_{j \leq n}$ (e.g., Arc Challenge) and extracting the relevant hidden states at the target layer. Since hidden states are available for each token position in a sequence for self-attention, we have $N = nT$, where T is the average prompt length. We then learn an approximate layer H_θ (rotors, LR, or BH) by minimizing

$$\min_\theta \sum_{i=1}^N (H_\theta x_i - y_i)^2,$$

where θ denotes the set of trainable parameters (e.g., bivector coefficients for rotors). Optimization is done via gradient descent using the Adam optimizer [Kingma and Ba, 2017].

We jointly replace the query, key, and value projections within an attention layer of a transformer block. In our experiments, we replace up to three such attention layers and evaluate the resulting model on downstream tasks of perplexity and accuracy metrics across various prompt datasets. When replacing multiple attention layers, say layers $I < J < K$, we train them sequentially in order: first I , then J , and finally K . For each layer, we first replace all earlier trained layers (e.g., I before J), and then extract the input-output data for training the new layer under this modified model. This is to ensure that each replacement layer is trained with respect to the distribution induced by preceding replacements. Also, whenever we replace layer L , we retrain the output linear projection W_o^L within the same attention block, using the same MSE and Adam optimizer for consistency.

Model	Key	Query	Value
LLaMa-3.2 1B	2048 → 512	2048 → 2048	2048 → 512
LLaMa-3.2 3B	3072 → 1024	3072 → 3072	3072 → 1024
Qwen-2.5 1.5B	1536 → 256	1536 → 1536	1536 → 256
Fox-1.0 1.6B	2048 → 512	2048 → 2048	2048 → 512

Table 5: Input/output hidden dimensions for key, query, and value projections in a single attention layer of different LLMs.

In Tab. 5, we summarize the input and output hidden dimension for different LLMs.

Rotor networks. We define the rotor-based transformation as:

$$\psi_{r,s}(x) \triangleq rxs^\dagger,$$

where $r, s \in \text{Spin}(n)$. Each rotor map is then composed as

$$\psi(x) \triangleq \sigma \left(\{ \psi_{r_{ij}, s_{ij}}(x^{I_i}) \mid i \in [c_1], j \in [c_2] \} \right),$$

where σ is a pooling operator applied over the outputs of individual rotor transformation $\psi_{r_{ij}, s_{ij}}$. More details are given in Subsection 4.2. As discussed, each rotor is parameterized by a small number of bivector coefficients that encode geometric rotations, leading to significantly fewer learnable parameters compared to dense or baseline layers. A rotor layer is constructed by stacking multiple rotor maps in depth and arranging them in parallel across width. For example, with width 2 and depth 3, the layer contains 6 rotor maps, each parameterized independently. In our experiments, to reduce computational cost, we use at most width 2 and depth 3 for a rotor layer, which along with any up and down projection needed that is done by the generalized version in 4.2 sums up to roughly 1000 scalar parameters per projection (i.e., per Q/K/V) layer for LLaMa-3.2 1B, compared to 1 – 4M in original dense layers.

Each rotor map is followed by a sequence of fixed (i.e., parameter-free) permutations, normalizations, and a nonlinearity. Since rotor sandwich products are grade-preserving (see Section B), we apply fixed permutations to enable interaction across grades and increase expressivity. We found that normalization improves training stability.

Hyperparameters such as depth, width, learning rate, and weight decay are selected via grid search; the final values along with the values we explored are listed in Tab. 6. All Clifford algebraic operations, including exponentiation of simple bivectors and sandwich products, are implemented entirely in PyTorch using the `torch_ga` library Alesiani, which supports differentiation. We modified several methods in this package to reduce memory usage. For example, the original package computes the geometric product using a very sparse three dimensional Cayley table of shape $2^n \times 2^n \times 2^n$ [Hitzer, 2013]. However, since we only require the geometric product between a pure rotor and a multivector when computing the sandwich product, we discard all but $1 + \binom{n}{2}$ parts of the third dimension, rather than keeping the full 2^n .

Low-rank approximations. We use low-rank (LR) approximation as one of our baselines, following prior work such as Hu et al. [2021]. Given a dense matrix $W \in \mathbb{R}^{d_{\text{out}} \times d_{\text{in}}}$, we approximate it as the product of two lower-dimensional matrices: $X \in \mathbb{R}^{d_{\text{out}} \times r}$ and $Y \in \mathbb{R}^{r \times d_{\text{in}}}$, such that

$$W \approx XY,$$

where $r \ll d_{\text{in}}, d_{\text{out}}$. This decomposition effectively constrains the rank of the approximation to at most r , capturing a low-rank subspace of the original operator. Low-rank approximations have

Method	Hyperparameter	Values Explored	Final Value
Rotor	Chunk Size	1024, 2048, 4096	2048
	Depth	1,2,3	1 or 3
	Width	1,2,3	1 or 2
	Nonlinearity	ReLU, PReLU, GELU	PReLU
	Normalization	true, false	true
	Permutations	true, false	true
	Learning rate	0.001, 0.005, 0.01, 0.05	0.05
	ℓ^2 weight decay	0.001, 0.01, 0.1, 0	0
	Batch size	16, 32, 64, 128, 256	64
Low-Rank (LR)	Cosine annealing	true, false	true
	Learning rate	0.001, 0.005, 0.01, 0.05	0.01
	ℓ^2 weight decay	0.001, 0.01, 0.1, 0	0
	Batch size	16, 32, 64, 128, 256	256
Block-Hadamard (BH)	Cosine annealing	true, false	true
	Block number	64	64
	Learning rate	0.001, 0.005, 0.01, 0.05	0.01
	ℓ^2 weight decay	0.001, 0.01, 0.1, 0	0
	Batch size	16, 32, 64, 128, 256	256
Cosine annealing	Cosine annealing	true, false	true

Table 6: Hyperparameter settings used for each method.

been shown to be effective in downstream tasks, especially when applied as additive fine-tuning modules to frozen large pre-trained weights. They are also computationally efficient, requiring only $\mathcal{O}(r(d_{\text{out}} + d_{\text{in}}))$ parameters and operations. In our experiments, we choose $r = 1$ and $r = 4$, and LR1 requires roughly $3 - 5 \times$ parameters than rotor layers. Hyperparameters are listed in Tab. 6.

Block-Hadamard approximations. We adopt the Block-Hadamard (BH) projection as another baseline. The idea is to alternate Hadamard transforms with learnable block-diagonal matrices, enabling a trade-off between expressivity and efficiency through the block size [Zeng et al., 2023]. Formally, it is defined as

$$W \approx \prod_{i=1}^m B_i H,$$

where each B_i is a learnable block-diagonal matrix with block size b , and H is a fixed Hadamard transform. This approximation requires only $\mathcal{O}(b \cdot \max(d_{\text{in}}, d_{\text{out}}))$ parameters, and can be interpreted as analogous to grouped convolutions followed by channel shuffling [Zhang et al., 2017]. The parameter m controls the depth of the transformation. In our experiments, we use $m = 1$ (i.e., BH1) to reduce parameter count as much as possible and match the scale of rotor-based models. Even with this minimal configuration, BH1 has $8\text{-}40 \times$ more parameters than rotors in the case of LLaMa-3.2 1B. Specifically, we use the approximation $W \approx BH$, where B is a block-diagonal matrix composed of n rectangular blocks, each of height $h = d_{\text{out}}/n$ and width $w = d_{\text{in}}/n$ for the number n of blocks. Hyperparameters are listed in Tab. 6.

Hyperparameters and model architecture of FMNIST experiments. We trained both dense and rotor-based MLPs under identical conditions. Each model consists of 2 hidden layers (either rotor or dense), followed by ReLU activations. All dense layers were replaced with rotor layers in our rotor variant, except for the final classification head. The dense layers had hidden dimension of 512, while the rotor layers used Cl(15) with width 3 and depth 1. We performed a search over learning rates $\eta \in (0.001, 0.1)$ and selected $\eta = 0.005$ for the rotor-based model and $\eta = 0.002$ for the dense baseline based on validation accuracy.

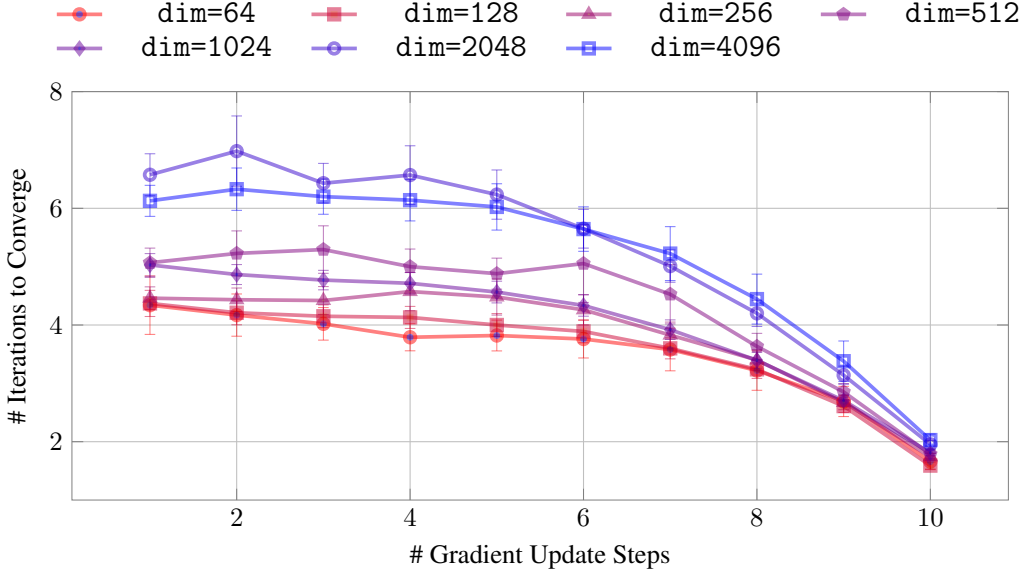


Figure 6: Number of iterations required by Alg 2 to converge within a tolerance of $\epsilon = 10^{-3}$, plotted against the number of gradient updates applied to the parameters of rotors (i.e., bivector coefficients). Results are averaged over 50 runs and simple bivectors in the invariant decomposition, with one standard deviation shown as error bars. The results demonstrate that warm-starting with previously learned singular vectors significantly accelerates convergence.

C.2 Computational Resources for Experiments

The experiments for each LLaMa-3.2 1B and Qwen-2.5 1.5B each took around 1500 GPU hours, Fox-1.0 1.6B around 1000 GPU hours, and LLaMa-3.2 3B around 500 GPU hours for a total of around 4500 GPU hours. This was spread across 8 NVIDIA A100 PCIe GPUs with 40 GBs of HBM2 memory. Total time of execution was around 3 weeks of run-time across all 8 GPUs.

A note on the execution time of the rotor gadget. We have not optimized the current code for speed or memory. At inference time, rotor layers are implemented as dense matrix multiplications. Therefore, its runtime scales with the depth of the rotor layer used in the replacement. In our experiments, we used hyperparameters of at most depth 2 and width 3; with an optimized implementation, this will result in at most $2\times$ slowdown, since width is trivially parallelizable.

It is important to note that this corresponds to a direct implementation—we currently do not leverage the block sparsity structure described in Section B.3, as current software support is quite limited. Custom kernels have recently become available to *batch* matrix-matrix multiplication of different dimensions, such as those available in `cublasGemmGroupedBatchedEx`, but our setting requires vector-matrix multiplication. We found that this is slower than performing the dense implementation, though performance is expected to improve significantly once specialized vector-matrix versions become available. While custom kernels such as `cublasSgemmStridedBatched` support batching matrix-matrix multiplication of the *same* dimension, their adaptation to rotors remains limited: even when applied to the parallel portions of the rotor gadget, they must operate sequentially on each block of the block sparse matrices. As a result, this gives a modest speedup, and there remains substantial room for further optimization.

D Additional Experimental Results

In Fig. 6, we report the number of iterations required by Alg. 2 to converge within a tolerance of $\epsilon = 10^{-3}$, as a function of the number of gradient updates applied to the rotors (i.e., bivector coefficients). Synthetic data was generated with random input and having output come from the rotation corresponding to a random bivector. Each gradient update step is towards learning that random bivector with MSE loss. As expected, higher-dimensional projections require more iterations to converge. Notably, warm-starting from previously learned singular values significantly reduces the convergence speed across all dimensions, supporting our claim in Section 4.1.

Model	Method	Key	Query	Value	Total
LLaMa-3.2 1B	Dense	1,048,576	4,194,304	1,048,576	6,291,456
	LR1	2,560	4,096	2,560	9,216
	LR4	10,240	16,384	10,240	36,864
	BH1	8,192	32,768	8,192	49,152
	Rotor	$\leq 1,080$	≤ 896	$\leq 1,080$	$\leq 3,056$
LLaMa-3.2 3B	Dense	3,145,728	9,437,184	3,145,728	15,728,640
	LR1	4,098	6,148	4,098	14,344
	LR4	16,384	24,576	16,384	57,344
	BH1	32,768	98,304	32,768	163,840
	Rotor	$\leq 1,080$	$\leq 1,120$	$\leq 1,080$	$\leq 3,280$
Qwen-2.5 1.5B	Dense	393,216	2,359,296	393,216	3,145,728
	LR1	1,792	3,072	1,792	6,656
	LR4	7,168	12,288	7,168	26,624
	BH1	4,096	24,576	4,096	32,768
	Rotor	≤ 904	≤ 896	≤ 904	$\leq 2,704$
Fox-1.0 1.6B	Dense	1,048,576	4,194,304	1,048,576	6,291,456
	LR1	2,560	4,096	2,560	9,216
	LR4	10,240	16,384	10,240	36,864
	BH1	8,192	32,768	8,192	49,152
	Rotor	$\leq 1,080$	≤ 896	$\leq 1,080$	$\leq 3,056$

Table 7: Number of parameters for key, query, and value projections in a single attention layer of each model, with the rightmost column showing their sum.

In Tab. 8, 9, and 10, we provide additional experimental results on Qwen-2.5 1.5B, LLaMa-3.2 3B, and Fox-1.0 1.6B [Hu et al., 2025], where a single attention layer is replaced by Rotor, LR1, LR4, or BH1 approximations. In Tab. 11, we provide averages for single and two-layer replacements for Fox-1-1.6B. The trends observed in the main paper persist: our rotor-based method consistently matches the baselines with significantly fewer parameters (see Tab. 7). These results further support our central claim: *linear layers can be synthesized from a small number of geometric primitives encoding rotations*.

Dataset	Method	One layer replaced (Layer index)													
		1	2	3	4	5	6	7	8	9	10	11	12	13	14
Wikitext2 (↓)	LR1	2.669	2.330	2.351	2.354	2.332	2.316	2.350	2.340	2.326	2.315	2.381	2.311	2.514	2.306
	LR4	2.635	2.320	2.334	2.343	2.320	2.310	2.335	2.331	2.318	2.310	2.368	2.307	2.456	2.306
	BH1	2.341	2.316	2.329	2.323	2.323	2.308	2.338	2.321	2.314	2.307	2.354	2.308	2.417	2.307
	Rotor	2.312	2.299	2.305	2.312	2.308	2.298	2.301	2.315	2.303	2.300	2.321	2.304	2.320	2.301
C4 (↓)	LR1	3.129	2.880	2.891	2.867	2.863	2.846	2.875	2.862	2.870	2.854	2.891	2.854	2.992	2.848
	LR4	3.007	2.880	2.890	2.869	2.862	2.846	2.873	2.862	2.867	2.854	2.888	2.853	2.939	2.848
	BH1	2.943	2.872	2.878	2.864	2.856	2.844	2.870	2.858	2.863	2.849	2.879	2.851	2.925	2.847
	Rotor	2.892	2.863	2.861	2.856	2.852	2.841	2.846	2.854	2.852	2.848	2.861	2.848	2.858	2.845
PTB (↓)	LR1	3.115	3.034	3.063	3.073	3.011	3.023	3.081	3.031	3.033	3.023	3.102	3.019	3.173	3.018
	LR4	3.110	3.021	3.063	3.055	3.006	3.015	3.076	3.030	3.028	3.012	3.078	3.018	3.150	3.017
	BH1	3.091	3.007	3.046	3.044	3.004	3.007	3.076	3.020	3.022	3.007	3.064	3.015	3.101	3.012
	Rotor	3.045	2.998	3.018	3.025	3.001	2.998	3.014	3.015	3.008	3.003	3.028	3.012	3.034	3.009
Arc Challenge (↑)	LR1	62.23	63.95	59.23	47.21	60.52	66.52	52.36	58.37	57.51	50.21	40.34	58.80	22.32	57.51
	LR4	59.66	62.66	64.81	54.94	60.94	66.09	56.22	62.66	66.09	58.37	55.79	61.37	9.01	58.80
	BH1	63.52	64.38	58.80	60.04	62.23	63.09	62.66	63.52	65.24	60.94	58.88	59.66	53.22	50.21
	Rotor	64.81	67.38	65.61	62.23	62.66	64.38	61.80	63.95	65.24	66.09	62.23	64.81	60.09	56.22
HellaSwag (↑)	LR1	36.00	47.00	45.00	46.67	50.00	51.00	50.33	44.00	17.33	36.00	46.00	52.67	31.33	20.00
	LR4	38.00	54.00	46.33	48.00	51.00	55.00	56.33	51.00	26.00	43.67	49.00	54.33	31.33	20.00
	BH1	45.67	48.00	46.00	48.33	48.67	50.67	51.67	52.33	38.33	44.67	48.00	51.33	24.33	32.67
	Rotor	50.67	53.00	53.67	52.33	52.00	55.33	57.00	54.67	48.67	55.33	51.00	57.00	51.33	32.00
Dataset	Method	One layer replaced (Layer index)													
		15	16	17	18	19	20	21	22	23	24	25	26	27	
Wikitext2 (↓)	LR1	2.317	2.304	2.314	2.317	2.323	2.316	2.331	2.316	2.309	2.301	2.409	2.300	2.316	
	LR4	2.317	2.304	2.314	2.317	2.323	2.316	2.331	2.316	2.309	2.301	2.409	2.300	2.316	
	BH1	2.313	2.301	2.314	2.316	2.320	2.311	2.311	2.315	2.309	2.300	2.398	2.297	2.309	
	Rotor	2.307	2.299	2.302	2.309	2.308	2.307	2.306	2.311	2.304	2.296	2.358	2.295	2.308	
C4 (↓)	LR1	2.866	2.854	2.900	2.860	2.869	2.866	2.898	2.883	2.861	2.866	2.872	2.854	2.860	
	LR4	2.865	2.851	2.899	2.859	2.868	2.866	2.889	2.866	2.856	2.851	2.858	2.853	2.858	
	BH1	2.862	2.847	2.856	2.858	2.867	2.862	2.872	2.857	2.854	2.849	2.852	2.850	2.853	
	Rotor	2.855	2.844	2.849	2.851	2.863	2.858	2.862	2.852	2.851	2.846	2.851	2.849	2.853	
PTB (↓)	LR1	3.025	3.003	3.020	3.021	3.036	3.019	3.086	3.010	3.014	3.012	3.019	3.061	3.098	
	LR4	3.024	3.003	3.026	3.018	3.034	3.017	3.017	3.010	3.015	2.997	3.017	3.012	3.024	
	BH1	3.017	3.000	3.008	3.014	3.029	3.012	3.010	3.009	3.011	2.995	3.015	3.005	3.016	
	Rotor	3.009	2.998	3.003	3.006	3.019	3.008	3.008	3.001	3.007	2.993	3.012	3.001	3.011	
Arc Challenge (↑)	LR1	41.20	65.24	27.90	65.24	68.24	16.31	47.64	67.38	66.95	65.67	65.24	66.09	66.52	
	LR4	31.76	69.1	58.37	65.24	68.24	16.31	47.64	67.38	66.95	65.67	65.24	66.09	66.52	
	BH1	49.79	68.67	48.50	62.23	62.24	42.49	48.93	65.24	67.81	64.39	65.31	65.79	65.24	
	Rotor	56.65	70.82	61.37	60.09	69.53	51.07	47.21	67.81	66.52	66.09	65.67	66.09	65.24	
HellaSwag (↑)	LR1	28.67	49.67	32.67	45.67	51.00	5.67	36.33	52.67	57.33	53.33	53.67	53.67	54.67	
	LR4	28.67	49.67	32.67	45.67	51.00	5.67	36.33	52.67	57.33	53.33	53.67	53.67	54.67	
	BH1	33.67	56.67	45.67	45.67	53.33	22.67	37.67	53.67	53.67	47.67	52.33	56.00	51.67	
	Rotor	42.67	55.00	49.33	51.33	52.67	18.67	35.00	51.00	56.67	54.00	54.33	54.00	56.67	

Table 8: Performance on log-PPL (↓) and accuracy (↑) when replacing **one attention layer** for layer indices 1–27 of Qwen-2.5 1.5B. Methods are Low-Rank ($r = 1$ and 4), BH1, and Rotor. Original log-PPL and accuracy are: Wikitext2 2.287, C4 2.834, PTB 2.985, Arc Challenge 66.09, Hellaswag 55.00.

Dataset	Method	One layer replaced (Layer index)													
		1	2	3	4	5	6	7	8	9	10	11	12	13	14
Wikitext2 (↓)	LR1	3.867	2.539	2.525	2.521	2.517	2.509	2.557	2.499	2.507	2.519	2.510	2.505	2.550	2.519
	LR4	3.389	2.514	2.512	2.501	2.510	2.492	2.531	2.488	2.494	2.497	2.501	2.500	2.510	2.503
	BH1	2.552	2.505	2.492	2.502	2.502	2.492	2.516	2.487	2.486	2.497	2.493	2.488	2.505	2.494
	Rotor	2.594	2.520	2.497	2.499	2.517	2.498	2.521	2.488	2.492	2.511	2.499	2.492	2.506	2.510
Wikitext2 (↓)	Method	15	16	17	18	19	20	21	22	23	24	25	26	27	
		2.501	2.487	2.481	2.473	2.487	2.484	2.477	2.479	2.487	2.489	2.490	2.479	2.519	
		2.497	2.485	2.477	2.471	2.480	2.479	2.471	2.467	2.480	2.474	2.471	2.471	2.503	
		2.484	2.479	2.476	2.471	2.472	2.475	2.466	2.469	2.477	2.476	2.475	2.469	2.482	
		2.488	2.481	2.477	2.471	2.476	2.478	2.466	2.471	2.482	2.484	2.482	2.477	2.496	

Table 9: Performance on log-PPL (↓) and accuracy (↑) when replacing **one attention layer** for layer indices 1–27 of LLaMa-3.2 3B. Methods are Low-Rank ($r = 1$ and 4), BH1, and Rotor. Original log-PPL is 2.460.

Dataset	Method	One layer replaced (Layer index)															
		1	2	3	4	5	6	7	8	9	10	11	12	13	14	15	16
Wikitext2 (↓)	LR1	2.645	2.573	2.549	2.535	2.531	2.546	2.550	2.533	2.581	2.540	2.557	2.546	2.538	2.538	2.536	2.546
	LR4	2.614	2.568	2.538	2.535	2.530	2.544	2.545	2.531	2.570	2.538	2.552	2.535	2.538	2.538	2.536	2.534
	BH1	2.633	2.548	2.545	2.534	2.530	2.545	2.544	2.531	2.577	2.536	2.550	2.538	2.537	2.537	2.534	2.532
	Rotor	2.544	2.542	2.541	2.532	2.529	2.538	2.540	2.530	2.537	2.533	2.549	2.536	2.534	2.531	2.531	2.531
C4 (↓)	LR1	2.997	2.915	2.879	2.877	2.877	2.891	2.884	2.878	2.889	2.886	2.876	2.884	2.874	2.881	2.878	2.875
	LR4	2.960	2.914	2.880	2.877	2.877	2.891	2.884	2.878	2.888	2.888	2.877	2.883	2.874	2.881	2.878	2.874
	BH1	2.991	2.901	2.875	2.878	2.876	2.891	2.881	2.878	2.889	2.879	2.874	2.876	2.872	2.879	2.877	2.872
	Rotor	2.924	2.901	2.875	2.876	2.876	2.890	2.881	2.878	2.882	2.878	2.873	2.876	2.872	2.878	2.876	2.871
PTB (↓)	LR1	3.359	3.270	3.222	3.231	3.226	3.225	3.222	3.231	3.279	3.233	3.229	3.268	3.232	3.237	3.231	3.279
	LR4	3.317	3.259	3.215	3.231	3.225	3.260	3.224	3.230	3.276	3.232	3.229	3.235	3.230	3.242	3.229	3.226
	BH1	3.318	3.230	3.214	3.230	3.224	3.259	3.224	3.229	3.277	3.231	3.228	3.234	3.230	3.241	3.227	3.227
	Rotor	3.283	3.229	3.212	3.229	3.224	3.257	3.223	3.228	3.255	3.229	3.228	3.232	3.228	3.234	3.225	3.225
Arc Challenge (↑)	LR1	31.76	31.33	33.05	42.06	42.49	47.64	36.48	44.64	22.75	41.63	24.03	39.48	39.91	20.17	21.03	29.18
	LR4	27.47	26.61	27.90	36.91	39.06	48.50	36.05	41.20	15.45	35.19	18.88	31.33	42.06	16.74	21.03	23.61
	BH1	34.33	21.46	28.33	32.19	38.20	45.06	26.61	42.49	11.59	36.48	14.16	21.89	46.78	24.89	25.75	9.44
	Rotor	27.04	21.03	26.18	23.61	30.47	36.48	29.18	39.91	22.32	31.33	13.30	22.32	31.76	28.33	24.46	18.45
HellaSwag (↑)	LR1	31.33	37.00	35.33	34.33	44.00	44.67	42.67	45.33	8.33	17.33	5.00	28.67	31.33	42.67	23.33	39.00
	LR4	35.67	36.67	25.00	33.00	42.67	43.33	43.00	44.67	6.33	19.00	4.33	26.67	31.33	41.33	18.67	39.33
	BH1	40.00	34.00	24.67	35.33	44.33	45.00	42.67	45.33	9.67	19.67	5.33	22.67	36.00	40.00	29.67	33.33
	Rotor	40.00	37.33	28.33	36.67	44.67	44.33	41.00	44.33	17.33	32.33	18.33	35.67	34.00	42.67	26.33	38.33
Dataset	Method	One layer replaced (Layer index)															
		17	18	19	20	21	22	23	24	25	26	27	28	29	30	31	
Wikitext2 (↓)	LR1	2.536	2.530	2.564	2.553	2.534	2.544	2.546	2.523	2.537	2.522	2.535	2.617	2.540	2.544	2.571	
	LR4	2.534	2.528	2.563	2.553	2.534	2.543	2.541	2.523	2.536	2.523	2.534	2.558	2.531	2.543	2.541	
	BH1	2.532	2.528	2.558	2.550	2.530	2.538	2.537	2.521	2.530	2.521	2.532	2.556	2.529	2.539	2.532	
	Rotor	2.531	2.527	2.531	2.548	2.529	2.538	2.534	2.521	2.529	2.521	2.531	2.553	2.528	2.537	2.531	
C4 (↓)	LR1	2.879	2.878	2.891	2.884	2.879	2.888	2.879	2.872	2.885	2.872	2.875	2.875	2.870	2.876	2.904	
	LR4	2.879	2.877	2.891	2.884	2.880	2.889	2.879	2.872	2.884	2.872	2.874	2.875	2.870	2.875	2.890	
	BH1	2.878	2.876	2.883	2.883	2.878	2.886	2.878	2.871	2.879	2.870	2.872	2.873	2.868	2.874	2.886	
	Rotor	2.877	2.875	2.881	2.883	2.878	2.885	2.877	2.871	2.879	2.870	2.872	2.874	2.868	2.874	2.883	
PTB (↓)	LR1	3.229	3.233	3.253	3.246	3.220	3.237	3.227	3.218	3.248	3.221	3.219	3.249	3.220	3.242	3.264	
	LR4	3.224	3.221	3.239	3.240	3.214	3.226	3.222	3.213	3.230	3.219	3.218	3.222	3.212	3.233	3.235	
	BH1	3.222	3.222	3.238	3.239	3.214	3.226	3.222	3.210	3.230	3.217	3.217	3.222	3.212	3.221	3.226	
	Rotor	3.221	3.220	3.232	3.238	3.213	3.225	3.220	3.210	3.228	3.216	3.217	3.220	3.211	3.220	3.223	
Arc Challenge (↑)	LR1	4.72	6.87	39.91	44.21	18.45	33.91	34.33	21.46	7.30	27.47	18.88	29.18	47.64	10.30	7.73	
	LR4	6.87	8.15	38.63	41.63	18.88	30.90	34.33	21.46	8.58	27.04	18.88	31.76	48.07	12.45	13.73	
	BH1	10.30	5.58	35.62	42.49	20.17	30.04	32.19	24.03	9.87	25.32	19.31	25.32	46.78	18.88	24.46	
	Rotor	20.17	18.88	25.32	33.91	21.03	30.04	26.61	24.46	11.59	26.18	21.46	24.89	45.49	19.74	24.46	
HellaSwag (↑)	LR1	27.33	26.33	42.33	47.33	41.33	37.00	37.67	32.00	23.67	40.00	34.67	46.67	47.33	28.67	12.00	
	LR4	25.00	28.33	41.00	46.33	40.00	37.00	38.67	32.33	26.67	40.67	36.33	44.33	46.00	31.33	28.00	
	BH1	28.67	27.67	42.33	47.67	44.00	40.67	38.33	34.67	27.33	39.67	36.67	42.33	47.00	32.33	36.67	
	Rotor	33.67	34.00	33.00	34.67	37.67	41.00	38.33	34.33	29.67	39.67	33.67	40.67	46.33	31.67	38.67	

Table 10: Performance on log-PPL (↓) and accuracy (↑) when replacing **one attention layer** for layer indices 1–31 results of Fox-1.0 1.6B. Methods are Low-Rank ($r = 1$ and 4), BH1, and Rotor. Original log-PPL and accuracy are: Wikitext2 2.517, C4 2.862, PTB 3.205, Arc Challenge 24.89, Hellaswag 38.33.

		Dataset	Method	Fox-1.0 1.6B	
				one	two
Log-PPL	Wikitext2	Original	Original	—	2.517
			LR1	2.550	2.589
			LR4	2.540	2.578
			BH1	2.538	2.573
	C4	Rotor	2.534	2.576	
			Original	—	2.862
			LR1	2.881	2.907
			LR4	2.880	2.901
Accuracy (%)	PTB	BH1	2.878	2.898	
			2.877	2.901	
			Original	—	3.205
			LR1	3.238	3.299
	HellaSwag	LR4	3.230	3.276	
			3.228	3.275	
			3.226	3.259	
			Rotor	3.226	3.259
Accuracy (%)	Arc Challenge	Original	Original	—	24.89
			LR1	29.03	26.40
			LR4	27.40	27.12
			BH1	26.77	31.42
	HellaSwag	Rotor	25.82	30.22	
			Original	—	38.33
			LR1	32.33	25.49
			LR4	32.41	24.40
Accuracy (%)	HellaSwag	BH1	33.92	27.73	
			35.14	32.87	
			Rotor	35.14	32.87

Table 11: Log-PPL (\downarrow) and accuracy (\uparrow) using original, Low-Rank ($r = 1$ or 4), BH1, and Rotor for 1–2 layer replacements on Fox-1.0 1.6B. One-layer results are averaged over all layers; two-layer results are averaged over five random selections. Red indicates best, blue second-best per setting.